Atmos. Chem. Phys. Discuss., 15, 33583–33629, 2015
www.atmos-chem-phys-discuss.net/15/33583/2015/
doi:10.5194/acpd-15-33583-2015


Atmospheric Chemistry and Physics Discussions



# Observationally-constrained carbonaceous aerosol source estimates for the Pearl River Delta area of China

**N. Li[1,2], T.-M. Fu[3], J. J. Cao[1,4], J. Y. Zheng[5], Q. Y. He[2], X. Long[1], Z. Z. Zhao[1], N. Y. Cao[6], J. S. Fu[7], and Y. F. Lam[8]**

[1]Key Lab of Aerosol Chemistry & Physics, SKLLQG, Institute of Earth Environment, Chinese Academy of Sciences, Xi'an, China
[2]Department of Atmospheric Sciences, National Taiwan University, Taipei, Taiwan, China
[3]Department of Atmospheric and Oceanic Sciences and Laboratory for Climate and Ocean–Atmosphere Studies, School of Physics, Peking University, Beijing, China
[4]Institute of Global Environmental Change, Xi'an Jiaotong University, Xi'an, China
[5]College of Environmental Science and Engineering, South China University of Technology, Guangzhou, China
[6]Particle Technology Laboratory, University of Minnesota, Minneapolis, Minnesota, USA
[7]Department of Civil and Environmental Engineering, University of Tennessee, Knoxville, Tennessee, USA
[8]School of Energy and Environment, City University of Hong Kong, Hong Kong, China







Received: 14 October 2015 – Accepted: 17 November 2015 – Published: 27 November 2015

Correspondence to: T.-M. Fu (mayfu@pku.edu.cn)

Published by Copernicus Publications on behalf of the European Geosciences Union.





ACPD
15, 33583–33629, 2015



## Abstract

We simulated elemental carbon (EC) and organic carbon (OC) aerosols over the Pearl River Delta (PRD) area of China and compared the results to seasonal surface measurements, with the aim of quantifying carbonaceous aerosol sources from a "top-down" perspective. Our regional model was driven by current-best estimates of PRD EC ($39.5\,Gg\,C\,yr^{-1}$) and OC ($32.8\,Gg\,C\,yr^{-1}$) emissions and included updated secondary organic aerosol formation pathways. The simulated annual mean EC and OC concentrations were 4.0 and $7.7\,\mu g\,C\,m^{-3}$, respectively, lower than the observed annual mean EC and OC concentrations (4.5 and $13.1\,\mu g\,C\,m^{-3}$, respectively). We used multiple regression to match the simulated EC against seasonal mean observations. The resulting top-down estimate for EC emission in the PRD area was $52.9 \pm 8.0\,Gg\,C\,yr^{-1}$. We estimated the OC emission in the PRD area to be $60.2 \pm 10.3\,Gg\,C\,yr^{-1}$, based on the top-down EC emission estimate and the primary OC/EC ratios derived from bottom-up statistics. Using these top-down emission estimates, the simulated average annual mean EC and OC concentrations were improved to 4.4 and $9.5\,\mu g\,C\,m^{-3}$, respectively, closer to the observations. Secondary sources accounted for 42 % of annual mean surface OC in our top-down simulations, with biogenic VOCs being the most important precursors.

## 1 Introduction

The Pearl River Delta (PRD) area of China (Fig. 1), including parts of the Guangdong Province surrounding the Pearl River estuary (hereafter referred to as the inner PRD), the Hong Kong Special Administrative Region (hereafter referred to as Hong Kong), and the Macau Special Administrative Region (hereafter referred to as Macau), has experienced severe air pollution of fine particulate matter ($PM_{2.5}$) in recent years (Chan and Yao, 2008; Liu et al., 2013). In particular, carbonaceous aerosols, including elemental carbon (EC) and organic carbon (OC) aerosols, account for 21–52 % of





ACPD
15, 33583–33629, 2015



the surface $PM_{2.5}$ mass in this area (Cao et al., 2003, 2004; Hagler et al., 2006; Ho et al., 2006; Hu et al., 2012). EC and primary OC (POC) are emitted directly into the atmosphere from incomplete combustion associated with anthropogenic and biomass burning activities. OC is also produced secondarily within the atmosphere (as secondary organic carbon, SOC) from gaseous organic precursors emitted by biogenic, anthropogenic, and biomass burning sources (Hallquist et al., 2009). Accurate quantification of these primary and secondary carbonaceous aerosol sources is paramount to effective air quality management in the PRD area.

Emission inventories are mostly constructed from the "bottom-up" using sectorial activity data and pollutant emission factors. Table 1 summarizes previous bottom-up estimations of PRD carbonaceous aerosol emissions. Total PRD EC emissions from anthropogenic and biomass burning activities were estimated to be 19.4–38.3 and 0.4–0.7 $Gg\,C\,yr^{-1}$, respectively. Total PRD OC emissions from anthropogenic and biomass burning activities were estimated to be 28.7–40.9 and 2.1–3.4 $Gg\,C\,yr^{-1}$, respectively (Streets et al., 2003b; Zhang et al., 2009; M. He et al., 2011; Zheng et al., 2012). The uncertainties of these bottom-up estimates are considerable, with 95 % confidence intervals (CI) ranging from 58 to 495 % (Streets et al., 2003b; Zhang et al., 2009; M. He et al., 2011; Zheng et al., 2012).

A few previous studies have used observations to constrain carbonaceous aerosol emissions for China at the national scale (Hakami et al., 2005; Kondo et al., 2011; Fu et al., 2012; X. Wang et al., 2013). Hakami et al. (2005) quantified East Asian black carbon (BC) emissions using BC measurements over South Korea, Japan, and the East China Sea during April 2001. They found that the East Asian domain-wide BC emission agreed well with the estimates of Streets et al. (2003a, b) (143 Gg C during April 2001), but sub-regional emission totals were underestimated for Japan and northeastern China and overestimated for southeastern China. Kondo et al. (2011) analyzed surface BC measurements at an island site in the East China Sea. They estimated Chinese annual BC emission to be 1.92 $Tg\,C\,yr^{-1}$, close to the estimate (1.81 $Tg\,C\,yr^{-1}$) by Zhang et al. (2009). X. Wang et al. (2013) analyzed BC observations at two Chinese ru-





ACPD
15, 33583–33629, 2015



ral sites, excluding measurements during high pollution events and those impacted by wet deposition. They estimated the Chinese annual BC emission to be 1.80 Tg C $yr^{-1}$, also similar to the estimate by Zhang et al. (2009). Fu et al. (2012), a forerunner to this current study, used model simulations and surface measurements at 10 Chinese rural and background sites to quantify Chinese annual EC and OC emissions. They estimated EC and OC emissions to be $3.05 \pm 0.78$ and $6.67 \pm 1.30$ Tg C $yr^{-1}$, respectively. To the best of our knowledge, there has not yet been a systematic quantification of PRD carbonaceous aerosol emissions using observational constraints.

Neither the contribution of SOC to total OC, nor the sources and formation pathways of SOC in the PRD area are well understood. Estimates of the secondary fraction of total OC in the PRD area ranged from 9 to 74 % with urban/rural and seasonal differences, but there are considerable inconsistencies (Cao et al., 2003, 2004; Ho et al., 2003; Hagler et al., 2006; Gnauk et al., 2008; Hu et al., 2008; L.-Y. He et al., 2011; X.-F. Huang et al., 2011; Hu et al., 2012; Ding et al., 2012). Hu et al. (2008) found that the summertime SOC in Hong Kong were mainly produced by biogenic monoterpenes and sesquiterpenes. In contrast, Ding et al. (2012) found that the SOC at a rural site in central PRD were mostly produced by anthropogenic aromatic precursors year-round. Regional models driven by bottom-up emission inventories for carbonaceous aerosols and organic gaseous precursors found biogenic precursors to be the main source of the simulated SOA (65–90 %) in the PRD area (Han et al., 2008; Jiang et al., 2012; Fu et al., 2012). However, these models also tend to underestimate PRD total OC by 30–60 % (Han et al., 2008; Jiang et al., 2012; Fu et al., 2012). Most of these models simulated SOA formation by the reversible partitioning of the semi-volatile oxidation products from anthropogenic and biogenic VOC precursors (Pankow, 1994; Odum et al., 1996). More recent modeling studies found that newly discovered pathways, such as the aqueous uptake of dicarbonyls (X.-H. Huang et al., 2011; Fu et al., 2012; Li et al., 2013) and the aging of semi-volatile and intermediate volatility organic compounds (S/IVOCs) (Guo et al., 2014; Matsui et al., 2014) may be important sources of SOC in the PRD area, potentially bridging the gap between simulated and observed OC.





ACPD
15, 33583–33629, 2015



In this study, we used a regional air quality model to simulate seasonal surface EC and OC concentrations in the PRD area for the year 2006. We drove the simulation using current-best bottom-up estimates for PRD carbonaceous aerosol emissions. We compared model results to seasonal surface observations at urban and rural sites to quantify the primary and secondary sources of PRD carbonaceous aerosols from a top-down perspective.

## 2 Simulations and observations

### 2.1 The CMAQ model

We used the CMAQ model (version 4.7.1) (Binkowski and Roselle, 2003; Byun and Schere, 2006) to simulate carbonaceous aerosols in the PRD area for the year 2006. CMAQ was driven by simulated meteorological fields from the Weather Research and Forecasting Model (WRF, version 3.2.1) (Skamarock et al., 2008). We simulated three nested domains covering East Asia, Southern China, and the PRD area, with horizontal resolutions of 27, 9, and 3 km, respectively (Fig. S1 in the Supplement). Vertical layers extended from the surface to 50 hPa (26 layers), with 17 layers in the bottom one km. Initial and boundary concentrations of chemical tracers were taken from the monthly mean outputs from a global chemical transport model (Fu et al., 2012). Our simulation was conducted for four 7 day periods in 2006 to represent the typical meteorological and emission conditions for each of the four seasons (4–10 January for winter, 14–20 April for spring, 24–30 July for summer, and 10–16 October for autumn). The model was initialized for the first day of each 7 day period. Results from the second to seventh day were analyzed.

Carbonaceous aerosols in the CMAQ model included EC and POC from anthropogenic and biomass burning emissions (Sect. 2.2), as well as SOC produced from organic gaseous precursors (described below). Carbonaceous aerosols were divided into Aitken and accumulation modes. Microphysical processes were simulated using





ACPD
15, 33583–33629, 2015



moment-based parameterizations (Binkowski and Roselle, 2003). All aerosols were subject to dry and wet deposition. Accumulation and coarse mode aerosols were assumed to be 100 % scavenged by cloud and rain water. The wet scavenging efficiency of Aitken mode aerosols in clouds were calculated as a function of air pressure, temperature, and cloud liquid water content (Byun and Schere, 2006).

We included in our CMAQ model three SOC formation pathways. The first two pathways were standard in the CMAQ model: (1) semi-volatile SOC formation by the reversible-partitioning of the semi-volatile oxidation products of VOC precursors (isoprene, monoterpenes, sesquiterpenes, long alkanes, and aromatics) onto preexisting OC (Pankow, 1994; Odum et al., 1996), and (2) non-volatile SOC formation via the oligomerization of semi-volatile SOC (Carlton et al., 2010), via the acid-enhanced oxidation of isoprene, and via low-$NO_x$ oxidation of aromatics (Ng et al., 2007; Surratt et al., 2007).

A third SOC formation pathway, involving the irreversible uptake of dicarbonyls by aqueous particles, was implemented into CMAQ and described in detail by Li et al. (2013). Briefly, glyoxal and methylglyoxal were produced by the gas-phase oxidation of isoprene, monoterpenes, propane, > $C_2$ alkenes, acetylene, benzene, toluene, xylenes, phenol, cresols, acetone, glycolaldehyde, and hydroxyacetone. Glyoxal and methylglyoxal were then irreversibly taken up by wet aerosols and cloud droplets with a reactive uptake coefficient $\gamma = 2.9 \times 10^{-3}$ (Liggio et al., 2005; Zhao et al., 2006). The surface area of wet aerosols was diagnosed using composition- and humidity-dependent hygroscopic growth factors (Kim et al., 1993; Whitby and McMurry, 1997). Cloud droplet surface area was diagnosed from the simulated liquid water content in the cloudy fraction of the model grid, assuming effective droplet radii of 10 and 6 µm for maritime and continental clouds, respectively. The Henry's Law Constants were updated to $4.19 \times 10^5\,\mathrm{M\,atm^{-1}}$ for glyoxal (Ip et al., 2009) and $3.2 \times 10^4\,\mathrm{M\,atm^{-1}}$ (Zhou and Mopper, 1990) for methylglyoxal. Li et al. (2013) simulated SOA production during a photochemical smog event in autumn 2009 and compared the results to aerosol mass spectrometry (AMS) measurements at a PRD urban site. They found that including the





ACPD
15, 33583–33629, 2015



dicarbonyl SOA pathway significantly improved the agreement between the simulated SOA and the observed oxygenated organic aerosol (OOA), both in terms of the concentrations and the correlations with sulfate (a secondary aerosol mainly produced in the aqueous phase).

Our model did not include SOC formation from the aging of S/IVOCs (Robinson et al., 2007). Recent modeling studies showed that including this aging process may increase the simulated SOA concentrations by approximately 0.5 $\mu g\,m^{-3}$ over the PRD area in autumn (Guo et al., 2014) and by approximately 3 $\mu g\,m^{-3}$ over southern China in spring (Matsui et al., 2014). Thus, our simulated SOC (Sect. 5) is likely biased low and we will discuss the impacts in Sect. 5. However, this potential underestimation of SOC does not affect our top-down quantification of primary carbonaceous aerosol emissions.

## 2.2 Emissions of EC, OC, and VOC precursors

We combined four current-best bottom-up emission inventories of EC, OC, and VOC precursors for the PRD area and the rest of East and South Asia to drive our simulation. Tables 2 and 3 summarize the bottom-up annual emissions estimates of carbonaceous aerosols and VOC precursors for the PRD area used in our simulation.

Anthropogenic EC and OC emissions for the inner PRD were taken from the inventory developed by Zheng et al. (2012) for the year 2009, which had a native resolution of 3 km and included emissions from power generation, industry, transportation, and residential activities. Activity data were collected from provincial yearbooks. Emission factors for residential combustion were obtained from Chinese measurements. EC and OC emissions from other sectors were estimated using $PM_{2.5}$ emission factors and EC and OC fractional abundance in $PM_{2.5}$. Anthropogenic EC and OC emissions for Hong Kong, Macau, and the rest of East and South Asia were taken from the inventory developed by Zhang et al. (2009) for the year 2006, which had a native resolution of 0.5°. We interpolated their emission fluxes to our nested domains. Emission factors were determined based on a combination of Chinese measurements and data from western studies. The residential emissions from the Zheng





ACPD
15, 33583–33629, 2015



et al. (2012) inventory were misrepresented in space. We spatially distributed the residential emissions from Zheng et al. (2012) using the spatial pattern from the inventory developed by Zhang et al. (2009). We applied diurnal (Q. Zhang, personal communication, 2012) and seasonal variations (Zheng et al., 2012; Zhang et al., 2009) to the PRD and Chinese anthropogenic emissions based on activity statistics. No seasonal and diurnal variations were applied to anthropogenic emissions outside China. The total annual anthropogenic EC emission for the PRD area was 38.9 $Gg\,C\,yr^{-1}$, including 25.7 $Gg\,C\,yr^{-1}$ from transportation, 7.2 $Gg\,C\,yr^{-1}$ from industry, 4.9 $Gg\,C\,yr^{-1}$ from residential sources, and 1.1 $Gg\,C\,yr^{-1}$ from power generation. Annual anthropogenic OC emission for the PRD area was 29.8 $Gg\,C\,yr^{-1}$, including 12.9 $Gg\,C\,yr^{-1}$ from transportation, 12.3 $Gg\,C\,yr^{-1}$ from residential sources, 3.8 $Gg\,C\,yr^{-1}$ from industry, and 0.8 $Gg\,C\,yr^{-1}$ from power generation. For both EC and OC, Hong Kong and Macao combined only contributed approximately 2 % of the total emissions from the entire PRD area. The uncertainties (95 % CI) for residential emissions in the inner PRD were 2.0–10.9 $Gg\,C\,yr^{-1}$ for EC and 5.5–24.8 $Gg\,C\,yr^{-1}$ for OC (Zheng et al., 2012). The uncertainties for other sectorial emissions in the inner PRD, while likely to be high, were not quantified in Zheng et al. (2012). Lei et al. (2011) analyzed the uncertainties of their EC and OC estimates for China. We used here their uncertainties (95 % CI) for industrial (±300 % for EC and ±365 % for OC), power generation (±50 % for EC and ±36 % for OC), and transportation (±91 % for EC and ±70 % for OC) sources for the inner PRD.

Biomass burning EC and OC emissions within the inner PRD were taken from the inventory developed by M. He et al. (2011) for the year 2006. The inventory had a resolution of 3 km and included emissions from field burning of agricultural residues and from wild fires. Activity data were from Chinese statistics. Emission factors were specific to Chinese and Asian biomass types (Cao et al., 2008; Li et al., 2009; Chang and Song, 2010). Biomass burning EC and OC emissions in Hong Kong, Macau, and the rest of East and South Asia were taken from the inventory by Streets et al. (2003b), representative of mid-1990s burning conditions at a native resolution of 1°. We interpo-





ACPD
15, 33583–33629, 2015



lated the emission fluxes to our nested domains. We applied seasonal variations to the inner PRD biomass burning emissions based on activity statistics (M. He et al., 2011). No seasonal variations were applied to biomass burning emissions outside of the inner PRD. A few Asian biomass burning emission inventories have been developed for more recent years (Song et al., 2010; Huang et al., 2012). However, since the PRD EC and OC measurements incorporated in this study were not sensitive to biomass burning sources outside of the PRD area (as will be shown in Sect. 4.1), the choice of biomass burning emission inventory outside of the PRD area does not heavily influence our top-down emission estimates (see discussion in Sect. 4.1). Annual biomass burning EC emission in the PRD area was 0.6 $Gg\,C\,yr^{-1}$, including 0.4 $Gg\,C\,yr^{-1}$ from field burning of rice straw and 0.2 $Gg\,C\,yr^{-1}$ from field burning of other residues. Annual biomass burning OC emission in the PRD area was 3.0 $Gg\,C\,yr^{-1}$, including 1.4 $Gg\,C\,yr^{-1}$ from field burning of rice straw, 1.4 $Gg\,C\,yr^{-1}$ from field burning of other residues, and 0.2 $Gg\,C\,yr^{-1}$ from forest fires. The 95 % CI for biomass burning source in inner PRD were 0.1–1.2 $Gg\,C\,yr^{-1}$ for EC and 1.1–8.4 $Gg\,C\,yr^{-1}$ for OC (M. He et al., 2011). Combined with anthropogenic emissions, we estimated the overall emission uncertainties (95 % CI) in the inner PRD to be ±161 % for EC and ±122 % for OC (see Table 2).

Figures 2 and 3 show the spatial distributions of the annual EC and OC emissions for the PRD area from the bottom-up inventories used to drive our simulation. For each sector, the spatial patterns of EC and OC emissions were similar owing to their common combustive origin. Industrial and power generation emissions were dotted in the inner PRD, reflecting the locations of factories and power plants. Transportation emissions were highest over downtown Guangzhou and Shenzhen, which are the two most populated cities in the PRD area. Biomass burning emissions were mostly over the rural agricultural areas around Guangzhou, Dongguan, Jiangmen, Huizhou, and Zhaoqing, reflecting the burning of crop residue for land clearing purposes (mostly in winter) (M. He et al., 2011).

Table 3 summarizes the PRD VOC emissions we used to drive our model. For the inner PRD, anthropogenic and biomass burning VOC emissions were taken from the





ACPD
15, 33583–33629, 2015



inventories developed by Zheng et al. (2009) and M. He et al. (2011), respectively. For Hong Kong, Macau, and the rest of East and South Asia, anthropogenic and biomass burning VOC emissions were taken from the inventories developed by Zhang et al. (2009) and Streets et al. (2003b), respectively. Biomass burning emissions of glyoxal, methylglyoxal, glycolaldehyde, and hydroxyacetone were scaled from biomass burning CO emissions following Fu et al. (2008). Biogenic VOC emissions were calculated using the MEGAN algorithm (Guenther et al., 2006), driven by meteorological fields simulated by WRF and land cover and vegetation data from MODIS. Annual isoprene and monoterpenes emissions over the PRD area were 221 and 157 $Gg\,yr^{-1}$ respectively. Figure 4 shows the spatial distributions of anthropogenic xylenes, biomass burning glyoxal, and biogenic isoprene emissions. Anthropogenic xylenes emissions were highest near city centers and along major highways, reflecting vehicular sources. Biomass burning glyoxal emissions were mostly over rural agricultural areas, reflecting the burning of crop residue. Biogenic isoprene emissions were highest over the forested areas in the northwestern and northeastern parts of the PRD area.

### 2.3 Seasonal surface measurements of carbonaceous aerosols

We needed seasonal carbonaceous aerosol measurements with sufficient spatiotemporal coverage and resolution to provide top-down constraints on the carbonaceous aerosol sources in the PRD area. There have been many individual, short-term carbonaceous aerosol measurements in the PRD area, but data from a single, consistent network of long-term measurements is not yet available. We compiled a database consisting of seasonal carbonaceous aerosol measurements from 11 studies conducted at 23 PRD locations, including 15 urban (non-roadside) locations and 8 rural locations, between the years 2000 and 2008 (Cao et al., 2003, 2004; Ho et al., 2003; Hagler et al., 2006; Gnauk et al., 2008; Hu et al., 2008; L.-Y. He et al., 2011; Hu et al., 2012; X.-F. Huang et al., 2011; K. F. Ho, unpublished data, 2012; J. Tao, unpublished data, 2012). Figure 1 shows the spatial distribution of the 23 locations. Table 4 lists the details of each location. The measurements compiled here involved a number of different





ACPD
15, 33583–33629, 2015



sampling and analysis techniques, but there is currently no way to compare them in a consistent manner. We summarized the techniques used in Table 4 (additional information in Sect. S1 in the Supplement) and noted that there may be inconsistencies.

To reflect the seasonal variation, we averaged the measurements for each of the four seasons: spring (March–May), summer (June–August), autumn (September–November), and winter (December, January, and February). Carbonaceous aerosol measurements were available at 9 locations in Hong Kong, including 6 urban locations (BU, CW, KT, YL, UST, and TW) and 3 rural locations (TC, HT, and TM). However, our model was unable to resolve the spatial variability due to the low resolution of the bottom-up emission inventory in Hong Kong. We averaged the seasonal measurements at the 9 locations in Hong Kong to represent hereafter a single urban site, HK. Table 5 summarizes the number of available measurements of urban and rural sites in the PRD area in each season. A total of 43 seasonal measurements (32 urban and 11 rural) were used in Sect. 4 to quantify PRD carbonaceous aerosol sources.

Table 4 shows the seasonal surface EC and OC concentration measurements incorporated in our database. The seasonal mean surface EC and OC concentrations in all urban and rural sites varied in the range of 1.4–13.3 and 5.7–38.4 $\mu g\,C\,m^{-3}$, respectively. These concentrations are similar to the seasonal means typically observed in Shanghai (1–33 $\mu g\,C\,m^{-3}$ for EC and 2–27 $\mu g\,C\,m^{-3}$ for OC; Ye et al., 2003; Feng et al., 2006, 2009; Chen et al., 2008; Hou et al., 2011; Cao et al., 2012, 2013; Geng et al., 2013) and Beijing (2–32 $\mu g\,C\,m^{-3}$ for EC and 6–41 $\mu g\,C\,m^{-3}$ for OC; He et al., 2001; Dan et al., 2004; Sun et al., 2004; Duan et al., 2006; Zhou et al., 2012; Zhang et al., 2013; Zhao et al., 2013). The highest seasonal mean surface concentrations were observed in winter for both EC and OC at all sites.

For the purpose of constraining OC sources, it is useful to quantify the POC and SOC concentrations in the observed total OC. However, there is currently no way to unambiguously separate the primary or secondary components in OC or OA measurements. Seven of the 11 measurement studies incorporated in our database quantified





ACPD
15, 33583–33629, 2015



POC and SOC using the EC tracer method:

$$SOC = OC - POC = OC - EC \times (POC/EC). \quad (1)$$

The POC/EC ratio in Eq. (1) can be estimated using several methods. Most studies adopted the seasonal or annual minimum observed OC/EC ratio as the POC/EC ratio (Cao et al., 2003, 2004; K. F. Ho unpublished data, 2012; J. Tao unpublished data, 2012), assuming that there was no SOC when the observed OC/EC ratio was at this minimum value. Alternatively, Hu et al. (2012) estimated the POC/EC ratio using the OC/EC value corresponding to a minimum correlation between SOC and EC. Both methods assumed that the POC/EC ratio remained constant during the period of observation, which may not be true if emission sources change.

Two AMF studies were incorporated in our database (X.-F. Huang et al., 2011; L.-Y. He et al., 2011). These studies applied the positive matrix factorization (PMF) technique on the high-resolution mass spectra and identified four OA components, including hydrocarbon-like OA (HOA), biomass burning OA (BBOA), semi-volatile oxygenated OA (SV-OOA), and low-volatile oxygenated OA (LV-OOA). We used the total oxygenated OA (SV-OOA + LV-OOA) as a surrogate for total SOA. We estimated the SOC mass using the OC/OM mass ratios observed by L.-Y. He et al. (2011) and X.-F. Huang et al. (2011). Finally, Hu et al. (2008) estimated total SOC mass using known SOA tracers from isoprene, monoterpenes, $\beta$-caryophyllene, and toluene.

Table 4 summarizes the seasonal mean surface SOC concentrations measured at 15 urban and rural sites. SOC concentrations ranged from 1.2–19.1 $\mu g\,C\,m^{-3}$ for urban sites and from 2.0–6.7 $\mu g\,C\,m^{-3}$ for rural sites. At all sites where observations were available, the fraction of SOC in total OC were higher in summer (57 %) and lower in winter (46 %), likely due to the stronger photochemistry and the higher biogenic precursor emissions in warmer seasons.





ACPD
15, 33583–33629, 2015



## 3 Simulated carbonaceous aerosols with bottom-up emissions

Figure 5 shows our simulated surface EC concentrations using the bottom-up emissions and compares them against the observations. The simulated annual mean EC concentration averaged over the urban and rural sites (sampled at sites where seasonal observations were available) was 4.0 $\mu g\,C\,m^{-3}$, 11 % lower than the observed annual mean concentration (4.5 $\mu g\,C\,m^{-3}$). Simulated seasonal EC concentrations ranged from 0.9–8.3 $\mu g\,C\,m^{-3}$ and were highest in winter and lowest in summer, consistent with the observations. The gap between simulated and observed seasonal EC concentrations were within ±2.0 $\mu g\,C\,m^{-3}$ for rural sites and within ±3.5 $\mu g\,C\,m^{-3}$ for urban sites, except at three industrial sites: HP, LG, and LH. The prevailing low-level wind over the PRD in autumn and winter is northeasterly, which transports regional pollutants from inner Mainland China to the PRD. Our model reproduced well the observed EC concentrations at the CH site at northern edge of the PRD area in autumn and winter, with biases less than ±0.7 $\mu g\,C\,m^{-3}$. In spring and summer, the prevailing low-level wind over the PRD is southeasterly (from the Pacific). The model was also able to reproduce the relatively lower EC concentrations at the HK site in spring and summer. These show that the model reasonably captured the regional EC background transported from inner Mainland China or from the Pacific into the PRD domain.

Figure 5 also shows the sectorial contributions to the simulated surface EC based on sensitivity simulations using the bottom-up emissions. Simulations using the bottom-up emission estimates indicated transportation to be the largest annual mean EC source for most urban (averaged 58 %) and rural (averaged 53 %) sites. The second largest annual mean EC source was industrial emissions (13 %), followed by residential emissions (9 %). Contributions to the annual mean surface EC from power generation (3 %) and biomass burning (1 %) were minor. The contribution of annual mean EC transported from outside of the PRD area averaged 17 % for all urban and rural sites.

Figure 6 shows our simulated surface OC concentrations using the bottom-up emissions and compared them against observations. The simulated annual mean OC con-





ACPD
15, 33583–33629, 2015



centration averaged over urban and rural sites (sampled at sites where seasonal observations were available) was 7.7 $\mu g\,C\,m^{-3}$, 41 % lower than the observed 13.1 $\mu g\,C\,m^{-3}$. Simulated seasonal OC concentrations ranged from 3.0–16.0 $\mu g\,C\,m^{-3}$ and were highest in autumn and lowest in summer, consistent with the observations. The simulated seasonal OC concentrations agreed well with observations at rural sites, with biases less than $\pm 6.5\,\mu g\,C\,m^{-3}$ and a normalized mean bias (NMB) of −20 %. However, the simulated seasonal OC concentrations were significantly lower than observations at most urban sites (biases up to $\pm 28\,\mu g\,C\,m^{-3}$, NMB = −45 %), except at SU and ZQ (NMB = −16 %). Our model reproduced well the observed POC concentrations at the CH site in autumn and winter (biases less than $\pm 1.1\,\mu g\,C\,m^{-3}$) and at the HK site in spring and summer (biases less than $\pm 1.1\,\mu g\,C\,m^{-3}$). These indicate that our model was able to capture the regional POC background transported from outside of the PRD area.

Figure 6 also shows the primary sectorial and secondary contributions to surface OC concentrations. Using the bottom-up emission, transport from outside of the PRD area was the most important primary OC source, contributing 17 % of the simulated annual mean surface OC at urban sites and 24 % of that at rural sites. PRD transportation was the second largest primary OC source, contributing 17 % averaged for all urban and rural sites, while other PRD sources (biomass burning, industry, power generation, and residential sources) combined to contribute 18 %. Moreover, SOC was an important component of PRD OC in all seasons, contributing 43 and 52 % of the simulated annual urban and rural mean surface OC, respectively. The contribution of SOC was particularly pronounced in summer (55 %) and autumn (50 %). Even in winter, SOC contributed 32 % of the simulated seasonal urban and rural mean surface OC.

Figure 7 shows the scatter plots of simulated vs. observed seasonal mean surface EC, OC, and POC concentrations at PRD sites. Using the bottom-up emission estimates, our simulations underestimated the EC seasonal mean observations (reduced major axis regression slope = 0.79), with moderate performance at capturing the spatiotemporal variability (correlation coefficient $r = 0.54$). For OC and POC, our model





ACPD
15, 33583–33629, 2015



also underestimated the seasonal mean observations, with regression slopes of 0.41 and 0.57, respectively. The model had little skill in capturing the spatiotemporal variability of the seasonal mean OC and POC observations ($r$ = 0.35 for OC and $r$ = 0.44 for POC).

## 4 Top-down estimates of carbonaceous aerosol emissions

### 4.1 Top-down EC emission estimates

Using observations as constraints, we derived top-down estimates on EC sources in the PRD area. We divided the sources of PRD surface EC into four parts: (1) anthropogenic transportation, (2) anthropogenic non-transportation (including industrial, power generation, and residential sources), (3) biomass burning, and (4) background EC transported from outside of the PRD area. The reason for representing the industrial, power generation, and residential sources as one combined non-transportation source was that the simulated EC contributions from these sources showed high spatial correlations ($r$ = 0.49–0.63) and the observations used in this study were not able to distinguish them. As discussed in Sect. 3, our model satisfactorily reproduced the seasonal regional background EC levels (EC transported from outside of the PRD area). Hence, we assumed that the simulated regional EC background levels were reasonable, and subtracted them from the seasonal observations. We used multiple regression to match the simulated EC contributions from each sector against seasonal mean observations at the 15 urban and rural sites. The multiple regression model is:

$$\boldsymbol{c}_{\text{obs}} - \boldsymbol{c}_{\text{background}} = \beta_1 \boldsymbol{c}_{\text{transportation}} + \beta_2 \boldsymbol{c}_{\text{non-transportation}} + \beta_3 \boldsymbol{c}_{\text{biomass}} + \boldsymbol{\varepsilon}. \quad (2)$$

In Eq. (2), $\boldsymbol{c}_{\text{obs}}$ is the vector of observed seasonal EC concentrations. $\boldsymbol{c}_{\text{background}}$ is the vector of simulated regional EC background contributed by sources from outside of the PRD area. $\boldsymbol{c}_{\text{transportation}}$, $\boldsymbol{c}_{\text{non-transportation}}$, and $\boldsymbol{c}_{\text{biomass}}$ are the vectors of simulated EC contributed from anthropogenic transportation, from anthropogenic non-transportation





ACPD
15, 33583–33629, 2015



(industrial, power generation, and residential sources), and from biomass burning sources, respectively. $\beta_1$, $\beta_2$, and $\beta_3$ are the domain-wide scalar scale factors required for these sources to best match the seasonal observations obtained from the multiple regression. $\boldsymbol{\varepsilon}$ is the regression model error vector. We further assumed that the bottom-up estimate for EC emissions from biomass burning activities was correct, setting $\beta_3 = 1$ and subtracting the simulated $\beta_3 \boldsymbol{c}_{\text{biomass}}$ from the right-hand-side of Eq. (2). The rationale for this assumption is two-fold. Firstly, the bottom-up estimate for biomass burning EC emissions was two orders of magnitude smaller than the emissions from anthropogenic activities (Table 2). Secondly, at least at the time and locations where EC measurements were available, our simulation using the bottom-up inventories showed that biomass burning contributed very little to surface EC concentrations (annual-average 1 % for all sites). The scale factor for transportation emissions ($\beta_1$) obtained from the multiple regression was 0.49, with a standard deviation of ±0.12 and a $p$ value of 0.007. The scale factor for the anthropogenic non-transportation sector ($\beta_2$) was 3.01, with a standard deviation of ±0.56 and a $p$ value $< 0.001$. The multiple regression explained 78 % of the observed variance (adjusted $R^2 = 0.78$).

Table 2 summarizes our top-down EC emission estimates. The estimated total EC emission from the PRD area was $52.9 \pm 8.0\,\text{Gg C yr}^{-1}$, including $39.7 \pm 7.4\,\text{Gg C yr}^{-1}$ from anthropogenic non-transportation sources, $12.6 \pm 3.1\,\text{Gg C yr}^{-1}$ from anthropogenic transportation source, and $0.6 \pm 0.8\,\text{Gg C yr}^{-1}$ from biomass burning source (unchanged from the bottom-up biomass burning emission inventory). The corresponding 95 % CI of total top-down estimated EC was ±30 %, calculated assuming normality for emission estimate probabilities. Our top-down total EC emission estimate is 34 % larger than the bottom-up estimate ($39.5\,\text{Gg C yr}^{-1}$).

### 4.2 Top-down OC emission estimates

We used two methods to estimate the PRD OC emissions. Firstly, we used the multiple regression technique to best-match the simulated POC against seasonal POC





ACPD
15, 33583–33629, 2015



observations (Table 4). The multiple regression model is:

$$\boldsymbol{c}_{\text{obs}} - \boldsymbol{c}_{\text{background}} = \gamma_1 \boldsymbol{c}_{\text{transportation}} + \gamma_2 \boldsymbol{c}_{\text{non-transportation}} + \gamma_3 \boldsymbol{c}_{\text{biomass}} + \boldsymbol{\varepsilon}. \quad (3)$$

In Eq. (3), $\boldsymbol{c}_{\text{obs}}$ is the vector of the observed seasonal POC concentrations. $\boldsymbol{c}_{\text{background}}$ is the vector of simulated regional POC background contributed by sources from outside the PRD area. $\boldsymbol{c}_{\text{transportation}}$, $\boldsymbol{c}_{\text{non-transportation}}$, and $\boldsymbol{c}_{\text{biomass}}$ are the vectors of the simulated POC contributions from anthropogenic transportation, from anthropogenic non-transportation, and from biomass burning sources, respectively. $\gamma_1$, $\gamma_2$, and $\gamma_3$ are the corresponding scalar scale factors for these sources. $\boldsymbol{\varepsilon}$ is the regression model error vector. We assumed that the simulated POC from the outside PRD and biomass burning sources were correct, for reasons similar to the case of EC (as discussed in Sect. 3). The multiple regression gave scale factors $\gamma_1 = 0.55$ and $\gamma_2 = 2.88$. The resulting top-down estimate for PRD OC emission was $58.8\,\text{Gg C yr}^{-1}$.

Alternatively, we used a "hybrid" approach to estimate the OC emissions. We used the coefficients $\beta_1$, $\beta_2$ and $\beta_3$ from the multiple regression analysis for EC emission in Eq. (2) to scale the bottom-up OC emission estimates. This is equivalent to combining the POC/EC emission ratios from bottom-up inventories with the observed EC constraints. The resulting estimated total OC emission was $60.2\,\text{Gg C yr}^{-1}$.

The estimated PRD OC emissions using the two methods were similar. We chose the second (hybrid approach) estimate for further discussion, because its uncertainties come from two traceable origins: (1) explicitly from the multiple regression analyses on EC observations, and (2) implicitly from the POC/EC emission ratios used in the bottom-up inventories. In contrast, the uncertainty of the first estimate depends on the uncertainty of estimating POC concentrations from total OC measurements, which is much harder to quantify. Using the hybrid approach, the total estimated OC emission in the PRD area was $60.2 \pm 10.3\,\text{Gg C yr}^{-1}$, including $50.9 \pm 9.5\,\text{Gg C yr}^{-1}$ from anthropogenic non-transportation sources, $6.3 \pm 1.5\,\text{Gg C yr}^{-1}$ from anthropogenic transportation source and $3.0 \pm 3.8\,\text{Gg C yr}^{-1}$ from biomass burning (unchanged from the bottom-up biomass burning emission inventory). The uncertainty (estimated based on





ACPD
15, 33583–33629, 2015



the 95 % CI of the EC multiple regression) of total top-down estimated OC was ±34 %. The top-down estimated total OC emission estimate was 84 % larger than the bottom-up estimate (32.8 Gg C $yr^{-1}$).

Figure 8 shows the spatial distributions of the top-down EC and OC emission estimates. EC and OC emissions were enhanced over the entire PRD domain, with largest emissions over the center of the PRD area. The difference between the top-down and the bottom-up emissions was mainly due to the increase of the anthropogenic non-transportation sources.

### 4.3 Evaluation of the top-down emission estimates

We simulated seasonal surface EC and OC using our top-down estimates of carbonaceous aerosol emissions to evaluate their performance. Figure 5 shows the spatial and temporal distributions of the simulated seasonal mean surface EC concentrations using the top-down emissions and compared them to the observations. Our model performance improved for most sites at all seasons (averaged NMB from −13 to −2 %) compared to the simulation using the bottom-up emissions. Simulated EC increased significantly at industrial sites (HP and LG), correcting the low-biases there. Simulated seasonal EC concentrations at downtown sites (at LW in spring, at SU in summer, at SCI in autumn, and at PKU in all seasons) decreased and were also closer to the observations. The simulated annual mean EC concentration using top-down emissions for urban and rural sites (sampled at sites where seasonal observations were available) was 4.4 µg C $m^{-3}$, only 3 % lower than the observed 4.5 µg C $m^{-3}$.

Figure 5 also shows the sectorial contributions to the simulated EC using our top-down emission estimates. Anthropogenic non-transportation activities became the largest source of EC at most sites year-round, contributing on average 62 % for urban sites and 56 % for rural sites. For the industrial sites HP and LG, the contributions of anthropogenic non-transportation sources increased significantly (79 % for HP and 57 % for LG) compared to the simulation using the bottom-up inventories (41 % for HP and 20 % for LG).





ACPD
15, 33583–33629, 2015



Figure 6 shows the simulated seasonal mean surface OC concentrations using the top-down emissions and compared them against the observations. The simulated OC concentrations increased at all sites year-round and were closer to the observations. The simulated annual mean OC for urban and rural sites (sampled at sites where seasonal observations were available) was 9.5 $\mu g\,C\,m^{-3}$, 27 % lower than the observed 13.1 $\mu g\,C\,m^{-3}$. Anthropogenic non-transportation sources were the main sources of OC for most sites year-round, contributing on average 42 % for urban sites and 30 % for rural sites. The contributions of anthropogenic non-transportation sources at the industrial sites (HP and LG) also increased significantly (60 % for HP and 37 % for LG) compared to the simulation using the bottom-up inventories (31 % for HP and 15 % for LG).

Figure 9 shows the spatial distributions of the simulated annual mean surface OC concentrations using the top-down emissions. The total simulated annual mean surface OC over the entire PRD domain was 7.9 $\mu g\,C\,m^{-3}$. Anthropogenic emissions of OC was the largest source of surface OC in our simulation, contributing 38 % (3.0 $\mu g\,C\,m^{-3}$) of the annual mean surface OC. Primary OC transported from outside of the PRD area contributed 18 % of the annual mean surface OC (1.4 $\mu g\,C\,m^{-3}$). Biomass burning source played a minor role in the annual mean surface OC (3 %, 0.2 $\mu g\,C\,m^{-3}$).

Figure 7 compares the overall model performances using the bottom-up and top-down simulations. Using the top-down EC emission estimates, the model's ability at reproducing the magnitude and the spatiotemporal variability of the EC observations were significantly improved (slope = 0.90, $r$ = 0.65). The model's performance at reproducing the magnitudes and spatiotemporal variability of POC and total OC were also improved using the top-down OC emission estimates, although to smaller extents (slope = 0.79 for POC and 0.51 for total OC; $r$ = 0.56 for POC and 0.50 for total OC)

We compared our top-down estimated carbonaceous aerosol emissions in the PRD area with previous studies (Table 1). Our anthropogenic EC emission estimate is 170 % larger than the estimation of Zhang et al. (2009) (19.4 $Gg\,C\,yr^{-1}$) and 37 % larger than that of Zheng et al. (2012) (38.3 $Gg\,C\,yr^{-1}$). Our anthropogenic OC (53.6 $Gg\,C\,yr^{-1}$) is





ACPD
15, 33583–33629, 2015



40 % larger than the estimation of Zhang et al. (2009) (40.9 Gg C $yr^{-1}$) and 99 % larger than that of Zheng et al. (2012) (28.7 Gg C $yr^{-1}$).

The gap of these individual bottom-up emission inventories could be caused by two possible reasons. First, previous studies usually like to adopt the middle value of emission factors from results of western measurements when the local data were not available. Zhang et al. (2009) and Zheng et al. (2012) estimated EC and OC emission factors in power generation, industrial, and mobile sources by $PM_{2.5}$ emission factors and mass ratios of EC and OC in $PM_{2.5}$. The $PM_{2.5}$ emission factors were based on a combination of domestic and western measurements (Zhang et al., 2007; Zhao et al., 2010), but the mass ratios were mostly from foreign studies (Bond et al., 2004; Kupiainen et al., 2004). However, previous aerosol source profile studies showed out that the mass ratios of EC and OC in Chinese $PM_{2.5}$ are often larger from those in western studies (He et al., 2006, 2008; Wang et al., 2009). Another reason may be that previous bottom-up estimates are generally considered to underestimate activity levels and/or overestimate emission control technology. For example, the removal efficiencies of BC and OC in power generations and industrial combustions were assumed the same as that of $PM_{2.5}$ in Zhang et al. (2009) and Zheng et al. (2012), although the efficiencies of submicron particles are expected to be lower than larger particles.

## 5 Secondary sources of OC in the PRD area

Finally, we quantified the secondary contributions to surface OC in the PRD area. Our total simulated annual mean surface SOC concentration averaged over 15 urban and rural sites was 3.5 µg C $m^{-3}$, 51 % lower than the observed 7.2 µg C $m^{-3}$. The model performance at simulating SOC was best in autumn (NMB = −12 %), followed by spring (NMB = −53 %), summer (NMB = −62 %), and winter (NMB = −78 %). The model performance at simulating annual mean SOC was better for rural sites (NMB = −32 %) than for urban sites (NMB = −57 %). Figure 6 shows that the simulated total OC using the top-down emission estimates agreed well with the observations at rural site





ACPD
15, 33583–33629, 2015



but still underestimated observations at urban sites. Figure 7 shows that this gap was mainly owing to low-biases in our simulated urban SOC. These findings indicate that our model may still be underestimating SOC from anthropogenic sources. Our model successfully reproduced the observed SOC for rural sites especially in warmer seasons (NMB = 0 % for autumn and −40 % for summer). This indicates that our model simulated the SOC from biogenic source reasonably well.

Figure 9 shows the contributions of different SOC formation pathways in our model. Semi- and non-volatile SOC formation combined contributed 1.7 $\mu g\,C\,m^{-3}$ to the annual mean surface OC. Aqueous uptake of dicarbonyl similarly contributed 1.6 $\mu g\,C\,m^{-3}$ to the annual surface mean OC. Both types of SOC were higher in the north-west of the PRD area, reflecting the impact of high biogenic VOC emissions. In addition, semi- and non-volatile SOC concentrations also had high values over city centers, reflecting the impact of anthropogenic VOC precursor emissions. Combined, secondary sources accounted for 42 % of annual mean surface OC over the PRD area in our model. The result is similar with previous modeling studies (30–40 %) (Jiang et al., 2012; Han et al., 2008) but potentially lower than observation constraints (35–74 %) (Cao et al., 2003, 2004; Ho et al., 2003; Hagler et al., 2006; Gnauk et al., 2008; Hu et al., 2008; L.-Y. He et al., 2011; Hu et al., 2012; X.-F. Huang et al., 2011; K. F. Ho, unpublished data, 2012; J. Tao, unpublished data, 2012) in the PRD area.

Table 3 summarizes the sources of surface SOC as simulated by our model using the top-down emission estimates. Biogenic VOC was the dominant source of SOC in our model, contributing 74 % of the simulated annual mean SOC. Isoprene and monoterpenes each contributed approximately half of the SOC from biogenic sources. Anthropogenic and biomass burning VOCs accounted for 25 and 1 % of the simulated annual mean SOC, respectively. Hu et al. (2008) found monoterpenes and $\beta$-caryophyllene to be the largest sources of summertime SOA in Hong Kong, while Ding et al. (2012) found aromatics accounted for 76–79 % of the identified SOC in central PRD in summer, autumn and winter. Both Hu et al. (2008) and Ding et al. (2012) were based on SOA tracer analyses. Using an emission-based box model, S. Wang et al. (2013)





ACPD
15, 33583–33629, 2015



showed that the sources of SOC in the PRD area was highly variable across locations and seasons due to the spatiotemporal variability of precursor emissions. They found monoterpenes to be the most important contributor in Hong Kong, while toluene and xylenes were more important in Guangzhou.

As discussed above, our model likely underestimated SOC from anthropogenic sources. This may be in part due to the omission of SOC formation via the aging of S/IVOCs (Guo et al., 2014; Matsui et al., 2014) in our model. Matsui et al. (2014) simulated OA in East Asia including the SOA formation from S/IVOCs. They found that including the aging processes of gaseous organic precursors (alkanes, olefins, aromatics, isoprene, monoterpene and sesquiterpene) could narrow, but not close, the gap between simulated and observed SOA in southern China (simulated SOA increased from 1 to 4 $\mu g\,m^{-3}$, but was still underestimated by 30–40 %) and greatly enhance the interaction of anthropogenic and biogenic sources (biogenic SOA enhanced by 45 %). However, Matsui et al. (2014) still found biogenic sources to be the largest contributor of SOA over southern China, consistent to our results.

## 6 Conclusions

We used a regional chemical model to simulate seasonal carbonaceous aerosol concentrations in the PRD area of China and compared the results to surface measurements, with the aim of quantifying PRD carbonaceous aerosol sources. We used a combination of several current bottom-up emission estimates for EC (39.5 $Gg\,C\,yr^{-1}$) and OC (32.8 $Gg\,C\,yr^{-1}$) to drive our simulation. SOC formation in our model takes place via reversible-partitioning of semi-volatile oxidation products from VOCs, non-volatile SOC formation, and aqueous uptake of dicarbonyls.

Using the bottom-up emission inventories, the simulated results were 11 and 41 % lower than the surface EC and OC observations at 15 urban and rural sites, respectively. We used multiple regression to match the simulated EC contributions from different sectors against seasonal mean observations at all urban and rural sites. The re-





ACPD
15, 33583–33629, 2015



sulting top-down estimate for PRD EC emissions is $52.9 \pm 8.0\,\mathrm{Gg\,C\,yr^{-1}}$. We combined the POC/EC ratios from bottom-up statistics and our top-down EC source estimate to constrain OC emissions. The resulting top-down estimate for PRD OC emission is $60.2 \pm 10.3\,\mathrm{Gg\,C\,yr^{-1}}$. The agreement between model results and observations is significantly improved in the simulation using our top-down emissions, compared to that using the bottom-up emissions. The simulated annual mean EC concentration using top-down emission averaged over all urban and rural sites is $4.4\,\mu\mathrm{g\,C\,m^{-3}}$, 3 % lower than the observed $4.5\,\mu\mathrm{g\,C\,m^{-3}}$. The simulated annual mean OC concentration using top-down emission averaged over all urban and rural sites is $9.5\,\mu\mathrm{g\,C\,m^{-3}}$, 27 % lower than the observed $13.1\,\mu\mathrm{g\,C\,m^{-3}}$. Applying the top-down emissions, the model is also able to better capture the observed seasonal EC and OC concentrations and their spatiotemporal variability.

Secondary sources account for 42 % of annual mean surface OC in our top-down simulation. The most important source for SOC in the PRD area is biogenic emissions (74 %), with isoprene (37 %) and monoterpenes (36 %) being the major precursors. Our findings are important for the understanding and management of air pollution in the PRD area.

**The Supplement related to this article is available online at doi:10.5194/acpd-15-33583-2015-supplement.**

*Acknowledgements.* This work was supported by the Ministry of Science and Technology of China (2014CB441303), the National Natural Science Foundation of China (41222035, 41175101), and the Open Fund of the State Key Laboratory of Loess and Quaternary Geology (SKLLQG1221).





ACPD
15, 33583–33629, 2015



## References


Binkowski, F. S. and Roselle, S. J.: Models-3 community multiscale air quality (CMAQ) model aerosol component 1. Model description, J. Geophys. Res., 108, 4183, doi:10.1029/2001jd001409, 2003.

Bond, T. C., Streets, D. G., Yarber, K. F., Nelson, S. M., Woo, J. H., and Klimont, Z.: A technology-based global inventory of black and organic carbon emissions from combustion, J. Geophys. Res., 109, D14203, doi:10.1029/2003jd003697, 2004.

Byun, D. and Schere, K. L.: Review of the governing equations, computational algorithms, and other components of the models-3 Community Multiscale Air Quality (CMAQ) modeling system, Appl. Mech. Rev., 59, 51–77, doi:10.1115/1.2128636, 2006.

Cao, G. L., Zhang, X. Y., Wang, Y. Q., and Zheng, F. C.: Estimation of emissions from field burning of crop straw in China, Chinese Sci. Bull., 53, 784–790, doi:10.1007/s11434-008-0145-4, 2008.

Cao, J. J., Lee, S. C., Ho, K. F., Zhang, X. Y., Zou, S. C., Fung, K., Chow, J. C., and Watson, J. G.: Characteristics of carbonaceous aerosol in Pearl River Delta Region, China during 2001 winter period, Atmos. Environ., 37, 1451–1460, doi:10.1016/s1352-2310(02)01002-6, 2003.

Cao, J. J., Lee, S. C., Ho, K. F., Zou, S. C., Fung, K., Li, Y., Watson, J. G., and Chow, J. C.: Spatial and seasonal variations of atmospheric organic carbon and elemental carbon in Pearl River Delta Region, China, Atmos. Environ., 38, 4447–4456, doi:10.1016/j.atmosenv.2004.05.016, 2004.

Cao, J. J., Shen, Z. X., Chow, J. C., Watson, J. G., Lee, S. C., Tie, X. X., Ho, K. F., Wang, G. H., and Han, Y. M.: Winter and summer $PM_{2.5}$ chemical compositions in fourteen Chinese cities, JAPCA J. Air Waste Ma., 62, 1214–1226, doi:10.1080/10962247.2012.701193, 2012.

Cao, J.-J., Zhu, C.-S., Tie, X.-X., Geng, F.-H., Xu, H.-M., Ho, S. S. H., Wang, G.-H., Han, Y.-M., and Ho, K.-F.: Characteristics and sources of carbonaceous aerosols from Shanghai, China, Atmos. Chem. Phys., 13, 803–817, doi:10.5194/acp-13-803-2013, 2013.

Carlton, A. G., Bhave, P. V., Napelenok, S. L., Edney, E. D., Sarwar, G., Pinder, R. W., Pouliot, G. A., and Houyoux, M.: Model representation of secondary organic aerosol in CMAQv4.7, Environ. Sci. Technol., 44, 8553–8560, doi:10.1021/es100636q, 2010.

Chan, C. K. and Yao, X.: Air pollution in mega cities in China, Atmos. Environ., 42, 1–42, doi:10.1016/j.atmosenv.2007.09.003, 2008.






ACPD
15, 33583–33629, 2015



Chang, D. and Song, Y.: Estimates of biomass burning emissions in tropical Asia based on satellite-derived data, Atmos. Chem. Phys., 10, 2335–2351, doi:10.5194/acp-10-2335-2010, 2010.

Chen, M. H., Li, D., Qian, H., Xiu, G. L., and Shen, T.: Study on chemical component of $PM_{2.5}$ in the atmosphere of Shanghai, J. Occup. Environ. Med., 25, 365–369, 2008.

Dan, M., Zhuang, G. S., Li, X. X., Tao, H. R., and Zhuang, Y. H.: The characteristics of carbonaceous species and their sources in $PM_{2.5}$ in Beijing, Atmos. Environ., 38, 3443–3452, doi:10.1016/j.atmosenv.2004.02.052, 2004.

Ding, X., Wang, X.-M., Gao, B., Fu, X.-X., He, Q.-F., Zhao, X.-Y., Yu, J.-Z., and Zheng, M.: Tracer-based estimation of secondary organic carbon in the Pearl River Delta, south China, J. Geophys. Res., 117, D05313, doi:10.1029/2011jd016596, 2012.

Duan, F. K., He, K. B., Ma, Y. L., Yang, F. M., Yu, X. C., Cadle, S. H., Chan, T., and Mulawa, P. A.: Concentration and chemical characteristics of $PM_{2.5}$ in Beijing, China: 2001–2002, Sci. Total Environ., 355, 264–275, doi:10.1016/j.scitotenv.2005.03.001, 2006.

Feng, J. L., Chan, C. K., Fang, M., Hu, M., He, L. Y., and Tang, X. Y.: Characteristics of organic matter in $PM_{2.5}$ in Shanghai, Chemosphere, 64, 1393–1400, doi:10.1016/j.chemosphere.2005.12.026, 2006.

Feng, Y. L., Chen, Y. J., Guo, H., Zhi, G. R., Xiong, S. C., Li, J., Sheng, G. Y., and Fu, J. M.: Characteristics of organic and elemental carbon in $PM_{2.5}$ samples in Shanghai, China, Atmos. Res., 92, 434–442, doi:10.1016/j.atmosres.2009.01.003, 2009.

Fu, T.-M., Jacob, D. J., Wittrock, F., Burrows, J. P., Vrekoussis, M., and Henze, D. K.: Global budgets of atmospheric glyoxal and methylglyoxal, and implications for formation of secondary organic aerosols, J. Geophys. Res., 113, D15303, doi:10.1029/2007jd009505, 2008.

Fu, T.-M., Cao, J. J., Zhang, X. Y., Lee, S. C., Zhang, Q., Han, Y. M., Qu, W. J., Han, Z., Zhang, R., Wang, Y. X., Chen, D., and Henze, D. K.: Carbonaceous aerosols in China: top-down constraints on primary sources and estimation of secondary contribution, Atmos. Chem. Phys., 12, 2725–2746, doi:10.5194/acp-12-2725-2012, 2012.

Geng, F. H., Hua, J., Mu, Z., Peng, L., Xu, X. H., Chen, R. J., and Kan, H. D.: Differentiating the associations of black carbon and fine particle with daily mortality in a Chinese city, Environ. Res., 120, 27–32, doi:10.1016/j.envres.2012.08.007, 2013.

Gnauk, T., Mueller, K., van Pinxteren, D., He, L.-Y., Niu, Y., Hu, M., and Herrmann, H.: Size-segregated particulate chemical composition in Xinken, Pearl River





ACPD
15, 33583–33629, 2015



Delta, China: OC/EC and organic compounds, Atmos. Environ., 42, 6296–6309, doi:10.1016/j.atmosenv.2008.05.001, 2008.
Guenther, A., Karl, T., Harley, P., Wiedinmyer, C., Palmer, P. I., and Geron, C.: Estimates of global terrestrial isoprene emissions using MEGAN (Model of Emissions of Gases and Aerosols from Nature), Atmos. Chem. Phys., 6, 3181–3210, doi:10.5194/acp-6-3181-2006, 2006.
Guo, X. S., Situ, S. P., Wang, X. M., Ding, X., Wang, X. M., Yan, C. Q., Li, X. Y., and Zheng, M.: Numerical Modeling Analysis of Secondary Organic Aerosol (SOA) Combined with the Ground-based Measurements in the Pearl River Delta Region, Environ. Sci., 35, 1654–1661, doi:10.13227/j.hjkx.2014.05.004, 2014 (in Chinese).
Hagler, G. S. W., Bergin, M. H., Salmon, L. G., Yu, J. Z., Wan, E. C. H., Zheng, M., Zeng, L. M., Kiang, C. S., Zhang, Y. H., Lau, A. K. H., and Schauer, J. J.: Source areas and chemical composition of fine particulate matter in the Pearl River Delta region of China, Atmos. Environ., 40, 3802–3815, doi:10.1016/j.atmosenv.2006.02.032, 2006.
Hakami, A., Henze, D. K., Seinfeld, J. H., Chai, T., Tang, Y., Carmichael, G. R., Sandu, A.: Adjoint inverse modeling of black carbon during the Asian Pacific Regional Aerosol Characterization Experiment, J. Geophys. Res., 110, D14301, doi:10.1029/2004JD005671, 2005.
Hallquist, M., Wenger, J. C., Baltensperger, U., Rudich, Y., Simpson, D., Claeys, M., Dommen, J., Donahue, N. M., George, C., Goldstein, A. H., Hamilton, J. F., Herrmann, H., Hoffmann, T., Iinuma, Y., Jang, M., Jenkin, M. E., Jimenez, J. L., Kiendler-Scharr, A., Maenhaut, W., McFiggans, G., Mentel, Th. F., Monod, A., Prévôt, A. S. H., Seinfeld, J. H., Surratt, J. D., Szmigielski, R., and Wildt, J.: The formation, properties and impact of secondary organic aerosol: current and emerging issues, Atmos. Chem. Phys., 9, 5155–5236, doi:10.5194/acp-9-5155-2009, 2009.
Han, Z. W., Zhang, R. J., Wang, Q. G., Wang, W., Cao, J. J., and Xu, J.: Regional modeling of organic aerosols over China in summertime, J. Geophys. Res., 113, D11202, doi:10.1029/2007jd009436, 2008.
He, K. B., Yang, F. M., Ma, Y. L., Zhang, Q., Yao, X. H., Chan, C. K., Cadle, S., Chan, T., and Mulawa, P.: The characteristics of $PM_{2.5}$ in Beijing, China, Atmos. Environ., 35, 4959–4970, doi:10.1016/s1352-2310(01)00301-6, 2001.
He, L.-Y., Hu, M., Huang, X. F., Zhang, Y. H., Yu, B. D., and Liu, D. Q.: Chemical characterization of fine particles from on-road vehicles in the Wutong tunnel in Shenzhen, China, Chemosphere, 62, 1565–1573, doi:10.1016/j.chemosphere.2005.06.051, 2006.





ACPD
15, 33583–33629, 2015



He, L.-Y., Hu, M., Zhang, Y. H., Huang, X. F., and Yao, T. T.: Fine particle emissions from on-road vehicles in the Zhujiang Tunnel, China, Environ. Sci. Technol., 42, 4461–4466, doi:10.1021/es7022658, 2008.
He, L.-Y., Huang, X. F., Xue, L., Hu, M., Lin, Y., Zheng, J., Zhang, R., and Zhang, Y.-H.: Submicron aerosol analysis and organic source apportionment in an urban atmosphere in Pearl River Delta of China using high-resolution aerosol mass spectrometry, J. Geophys. Res., 116, D12304, doi:10.1029/2010jd014566, 2011.
He, M., Zheng, J., Yin, S., and Zhang, Y.: Trends, temporal and spatial characteristics, and uncertainties in biomass burning emissions in the Pearl River Delta, China, Atmos. Environ., 45, 4051–4059, doi:10.1016/j.atmosenv.2011.04.016, 2011.
Ho, K. F., Lee, S. C., Chan, C. K., Yu, J. C., Chow, J. C., and Yao, X. H.: Characterization of chemical species in $PM_{2.5}$ and $PM_{10}$ aerosols in Hong Kong, Atmos. Environ., 37, 31–39, doi:10.1016/s1352-2310(02)00804-x, 2003.
Ho, K. F., Lee, S. C., Cao, J. J., Li, Y. S., Chow, J. C., Watson, J. G., and Fung, K.: Variability of organic and elemental carbon, water soluble organic carbon, and isotopes in Hong Kong, Atmos. Chem. Phys., 6, 4569–4576, doi:10.5194/acp-6-4569-2006, 2006.
Hou, B., Zhuang, G. S., Zhang, R., Liu, T. N., Guo, Z. G., and Chen, Y.: The implication of carbonaceous aerosol to the formation of haze: revealed from the characteristics and sources of OC/EC over a mega-city in China, J. Hazard. Mater., 190, 529–536, doi:10.1016/j.jhazmat.2011.03.072, 2011.
Hu, D., Bian, Q., Li, T. W. Y., Lau, A. K. H., and Yu, J. Z.: Contributions of isoprene, monoterpenes, beta-caryophyllene, and toluene to secondary organic aerosols in Hong Kong during the summer of 2006, J. Geophys. Res., 113, D22206, doi:10.1029/2008jd010437, 2008.
Hu, W. W., Hu, M., Deng, Z. Q., Xiao, R., Kondo, Y., Takegawa, N., Zhao, Y. J., Guo, S., and Zhang, Y. H.: The characteristics and origins of carbonaceous aerosol at a rural site of PRD in summer of 2006, Atmos. Chem. Phys., 12, 1811–1822, doi:10.5194/acp-12-1811-2012, 2012.
Huang, X., Li, M. M., Li, J. F., and Song, Y.: A high-resolution emission inventory of crop burning in fields in China based on MODIS Thermal anomalies/fire products, Atmos. Environ., 50, 9–15, doi:10.1016/j.atmosenv.2012.01.017, 2012.
Huang, X.-F., He, L.-Y., Hu, M., Canagaratna, M. R., Kroll, J. H., Ng, N. L., Zhang, Y.-H., Lin, Y., Xue, L., Sun, T.-L., Liu, X.-G., Shao, M., Jayne, J. T., and Worsnop, D. R.: Characterization of submicron aerosols at a rural site in Pearl River Delta of China using an Aero-





ACPD
15, 33583–33629, 2015



dyne High-Resolution Aerosol Mass Spectrometer, Atmos. Chem. Phys., 11, 1865–1877, doi:10.5194/acp-11-1865-2011, 2011.
Huang, X.-H., Ip, H. S., and Yu, J. Z.: Secondary organic aerosol formation from ethylene in the urban atmosphere of Hong Kong: a multiphase chemical modeling study, J. Geophys. Res., 116, D03206, doi:10.1029/2010jd014121, 2011.
Ip, H. S. S., Huang, X. H. H., and Yu, J. Z.: Effective Henry's law constants of glyoxal, glyoxylic acid, and glycolic acid, Geophys. Res. Lett., 36, L01802, doi:10.1029/2008gl036212, 2009.
Jiang, F., Liu, Q., Huang, X. X., Wang, T. J., Zhuang, B. L., and Xie, M.: Regional modeling of secondary organic aerosol over China using WRF/Chem, J. Aerosol Sci., 43, 57–73, doi:10.1016/j.jaerosci.2011.09.003, 2012.
Kim, Y. P., Seinfeld, J. H., and Saxena, P.: Atmospheric gas aerosol equilibrium 1. thermodynamic model, Aerosol Sci. Tech., 19, 157–181, doi:10.1080/02786829308959628, 1993.
Kondo, Y., Oshima, N., Kajino, M., Mikami, R., Moteki, N., Takegawa, N., Verma, R. L., Kajii, Y., Kato, S., and Takami, A.: Emissions of black carbon in East Asia estimated from observations at a remote site in the East China Sea, J. Geophys. Res., 116, D16201, doi:10.1029/2011jd015637, 2011.
Kupiainen, K. and Klimont, Z.: Primary emissions of submicron and carbonaceous particles in Europe and the potential for their control, Interim report, IR-04-079, International Institute for Applied Systems Analysis, Laxenburg, Austria, 115 pp., 2004.
Lei, Y., Zhang, Q., He, K. B., and Streets, D. G.: Primary anthropogenic aerosol emission trends for China, 1990–2005, Atmos. Chem. Phys., 11, 931–954, doi:10.5194/acp-11-931-2011, 2011.
Li, N., Fu, T.-M., Cao, J., Lee, S., Huang, X.-F., He, L.-Y., Ho, K.-F., Fu, J. S., and Lam, Y.-F.: Sources of secondary organic aerosols in the Pearl River Delta region in fall: contributions from the aqueous reactive uptake of dicarbonyls, Atmos. Environ., 76, 200–207, doi:10.1016/j.atmosenv.2012.12.005, 2013.
Li, X., Wang, S., Duan, L., Hao, J., and Nie, Y.: Carbonaceous aerosol emissions from household biofuel combustion in China, Environ. Sci. Technol., 43, 6076–6081, doi:10.1021/es803330j, 2009.
Liggio, J., Li, S. M., and McLaren, R.: Reactive uptake of glyoxal by particulate matter, J. Geophys. Res., 110, D10304, doi:10.1029/2004jd005113, 2005.





ACPD
15, 33583–33629, 2015



Liu, H., Wang, X. M., Pang, J. M., and He, K. B.: Feasibility and difficulties of China's new air quality standard compliance: PRD case of $PM_{2.5}$ and ozone from 2010 to 2025, Atmos. Chem. Phys., 13, 12013–12027, doi:10.5194/acp-13-12013-2013, 2013.

Matsui, H., Koike, M., Kondo, Y., Takami, A., Fast, J. D., Kanaya, Y., and Takigawa, M.: Volatility basis-set approach simulation of organic aerosol formation in East Asia: implications for anthropogenic–biogenic interaction and controllable amounts, Atmos. Chem. Phys., 14, 9513–9535, doi:10.5194/acp-14-9513-2014, 2014.

Ng, N. L., Kroll, J. H., Chan, A. W. H., Chhabra, P. S., Flagan, R. C., and Seinfeld, J. H.: Secondary organic aerosol formation from *m*-xylene, toluene, and benzene, Atmos. Chem. Phys., 7, 3909–3922, doi:10.5194/acp-7-3909-2007, 2007.

Odum, J. R., Hoffmann, T., Bowman, F., Collins, D., Flagan, R. C., and Seinfeld, J. H.: Gas/particle partitioning and secondary organic aerosol yields, Environ. Sci. Technol., 30, 2580–2585, doi:10.1021/es950943+, 1996.

Pankow, J. F.: An absorption model of gas/particle partitioning of organic compounds in the atmosphere, Atmos. Environ., 28, 185–188, doi:10.1016/1352-2310(94)90093-0, 1994.

Robinson, A. L., Donahue, N. M., Shrivastava, M. K., Weitkamp, E. A., Sage, A. M., Grieshop, A. P., Lane, T. E., Pierce, J. R., and Pandis, S. N.: Rethinking organic aerosols: semivolatile emissions and photochemical aging, Science, 315, 1259–1262, doi:10.1126/science.1133061, 2007.

Skamarock, W. C., Klemp, J. B., Dudhia, J., Gill, D. O., Barker, D. M., Duda, M. G., Huang, X. Y., Wang, W., and Powers, J. G.: A description of the advanced research WRF version 3, NCAR Tech Notes-475+STR, 2008.

Song, Y., Chang, D., Liu, B., Miao, W., Zhu, L., and Zhang, Y.: A new emission inventory for nonagricultural open fires in Asia from 2000 to 2009, Environ. Res. Lett., 5, 014014, doi:10.1088/1748-9326/5/1/014014, 2010.

Streets, D. G., Bond, T. C., Carmichael, G. R., Fernandes, S. D., Fu, Q., He, D., Klimont, Z., Nelson, S. M., Tsai, N. Y., Wang, M. Q., Woo, J. H., and Yarber, K. F.: An inventory of gaseous and primary aerosol emissions in Asia in the year 2000, J. Geophys. Res., 108, 8809, doi:10.1029/2002jd003093, 2003a.

Streets, D. G., Yarber, K. F., Woo, J. H., and Carmichael, G. R.: Biomass burning in Asia: annual and seasonal estimates and atmospheric emissions, Global Biogeochem. Cy., 17, 1099, doi:10.1029/2003gb002040, 2003b.





ACPD
15, 33583–33629, 2015



Sun, Y. L., Zhuang, G. S., Ying, W., Han, L. H., Guo, J. H., Mo, D., Zhang, W. J., Wang, Z. F., and Hao, Z. P.: The air-borne particulate pollution in Beijing – concentration, composition, distribution and sources, Atmos. Environ., 38, 5991–6004, doi:10.1016/j.atmosenv.2004.07.009, 2004.

Surratt, J. D., Lewandowski, M., Offenberg, J. H., Jaoui, M., Kleindienst, T. E., Edney, E. O., and Seinfeld, J. H.: Effect of acidity on secondary organic aerosol formation from isoprene, Environ. Sci. Technol., 41, 5363–5369, doi:10.1021/es0704176, 2007.

Wang, S., Wu, D., Wang, X.-M., Fung, J. C.-H., and Yu, J. Z.: Relative contributions of secondary organic aerosol formation from toluene, xylenes, isoprene, and monoterpenes in Hong Kong and Guangzhou in the Pearl River Delta, China: an emission-based box modeling study, J. Geophys. Res., 118, 507–519, doi:10.1029/2012jd017985, 2013.

Wang, S. X., Zhao, X. J., Li, X. H., Wei, W., and Hao, J. M.: Emission Characteristics of fine particles from grate firing boilers, Environ. Sci. (in Chinese), 30, 963–968, 0250-3301(2009)04-0963-06, 2009.

Wang, X., Wang, Y. X., Hao, J. M., Kondo, Y., Irwin, M., Munger, J. W., and Zhao, Y. J.: Top-down estimate of China's black carbon emissions using surface observations: sensitivity to observation representativeness and transport model error, J. Geophys. Res., 118, 5781–5795, doi:10.1002/jgrd.50397, 2013.

Whitby, E. R. and McMurry, P. H.: Modal aerosol dynamics modeling, Aerosol Sci. Tech., 27, 673–688, doi:10.1080/02786829708965504, 1997.

Ye, B. M., Ji, X. L., Yang, H. Z., Yao, X. H., Chan, C. K., Cadle, S. H., Chan, T., and Mulawa, P. A.: Concentration and chemical composition of $PM_{2.5}$ in Shanghai for a 1 year period, Atmos. Environ., 37, 499–510, doi:10.1016/s1352-2310(02)00918-4, 2003.

Zhang, Q., Streets, D. G., He, K., and Klimont, Z.: Major components of China's anthropogenic primary particulate emissions, Environ. Res. Lett., 2, 045027, doi:10.1088/1748-9326/2/4/045027, 2007.

Zhang, Q., Streets, D. G., Carmichael, G. R., He, K. B., Huo, H., Kannari, A., Klimont, Z., Park, I. S., Reddy, S., Fu, J. S., Chen, D., Duan, L., Lei, Y., Wang, L. T., and Yao, Z. L.: Asian emissions in 2006 for the NASA INTEX-B mission, Atmos. Chem. Phys., 9, 5131–5153, doi:10.5194/acp-9-5131-2009, 2009.

Zhang, R., Jing, J., Tao, J., Hsu, S.-C., Wang, G., Cao, J., Lee, C. S. L., Zhu, L., Chen, Z., Zhao, Y., and Shen, Z.: Chemical characterization and source apportionment of $PM_{2.5}$ in





ACPD
15, 33583–33629, 2015



Beijing: seasonal perspective, Atmos. Chem. Phys., 13, 7053–7074, doi:10.5194/acp-13-7053-2013, 2013.
Zhao, J., Levitt, N. P., Zhang, R., and Chen, J.: Heterogeneous reactions of methylglyoxal in acidic media: implications for secondary organic aerosol formation, Environ. Sci. Technol., 40, 7682–7687, doi:10.1021/es060610k, 2006.
Zhao, P. S., Dong, F., He, D., Zhao, X. J., Zhang, X. L., Zhang, W. Z., Yao, Q., and Liu, H. Y.: Characteristics of concentrations and chemical compositions for $PM_{2.5}$ in the region of Beijing, Tianjin, and Hebei, China, Atmos. Chem. Phys., 13, 4631–4644, doi:10.5194/acp-13-4631-2013, 2013.
Zhao, Y., Wang, S., Nielsen, C. P., Li, X., and Hao, J.: Establishment of a database of emission factors for atmospheric pollutants from Chinese coal-fired power plants, Atmos. Environ., 44, 1515–1523, doi:10.1016/j.atmosenv.2010.01.017, 2010.
Zheng, J. Y., Shao, M., Che, W. W., Zhang, L. J., Zhong, L. J., Zhang, Y. H., and Streets, D. G.: Speciated VOC Emission inventory and spatial patterns of ozone formation potential in the Pearl River Delta, China, Environ. Sci. Technol., 43, 8580–8586, doi:10.1021/es901688e, 2009.
Zheng, J. Y., He, M., Shen, X. L., Yin, S. S., and Yuan, Z. B.: High resolution of black carbon and organic carbon emissions in the Pearl River Delta region, China, Sci. Total Environ., 438, 189–200, doi:10.1016/j.scitotenv.2012.08.068, 2012.
Zhou, J. M., Zhang, R. J., Cao, J. J., Chow, J. C., and Watson, J. G.: Carbonaceous and ionic components of atmospheric fine particles in Beijing and their impact on atmospheric visibility, Aerosol Air Qual. Res., 12, 492–502, doi:10.4209/aaqr.2011.11.0218, 2012.
Zhou, X. L. and Mopper, K.: Apparent partition-coefficients of 15 carbonyl-compounds between air and seawater and between air and fresh-water – implications for air sea exchange, Environ. Sci. Technol., 24, 1864–1869, doi:10.1021/es00082a013, 1990.





ACPD
15, 33583–33629, 2015



**Table 1.** Comparison of recent estimates for carbonaceous aerosol emissions in the PRD area.

| | Year | EC (Gg C yr$^{-1}$) | | OC (Gg C yr$^{-1}$) | |
|---|---|---|---|---|---|
| | | Anthropogenic* | Biomass burning | Anthropogenic* | Biomass burning |
| Streets et al. (2003b) | 2000 | – | 0.7 | – | 3.4 |
| Zhang et al. (2009) | 2006 | 19.4 | – | 40.9 | – |
| M. He et al. (2011) | 2006 | – | 0.6 | – | 3.0 |
| Zheng et al. (2012) | 2009 | 38.3 | 0.4 | 28.7 | 2.1 |
| This work | 2006 | 52.3 | 0.6 | 57.2 | 3.0 |

* Including emissions from industry, power generation, transportation, and residential activities.





ACPD
15, 33583–33629, 2015



**Table 2.** PRD carbonaceous aerosol emissions: bottom-up estimates used to drive our model and top-down estimates obtained from this study.

| Source sectors | EC ($Gg\,C\,yr^{-1}$) | | OC ($Gg\,C\,yr^{-1}$) | |
|---|---|---|---|---|
| | Bottom-up | Top-down[d] | Bottom-up | Top-down[d] |
| Anthropogenic | 38.9 | 52.3 ± 8.0 (±25 %) | 29.8[a] | 57.2 ± 9.6 (±33 %) |
| Industry | 7.2[a] | 39.7 ± 7.4 (±37 %) | 3.8[a] | 50.9 ± 9.5 (±37 %) |
| Power generation | 1.1[a] | | 0.8[a] | |
| Residential sources | 4.9[a] | | 12.3[a] | |
| Transportation | 25.7[a] | 12.6 ± 3.1 (±48 %) | 12.9[a] | 6.3 ± 1.5 (±48 %) |
| Biomass burning | 0.6[b] | 0.6 ± 0.8 (±133 %) | 3.0[b] | 3.0 ± 3.8 (±128 %) |
| Total | 39.5 (±161 %)[c] | 52.9 ± 8.0 (±30 %) | 32.8 (±122 %)[c] | 60.2 ± 10.3 (±34 %) |

[a] From Zheng et al. (2012) for the inner PRD and from Zhang et al. (2009) for Hong Kong and Macau. The uncertainties (represented as 95 % confidence intervals, CI) for residential emissions in the Zheng et al. (2012) inventory were 2.0–10.9 $Gg\,C\,yr^{-1}$ for EC and 5.5–24.8 $Gg\,C\,yr^{-1}$ for OC. The uncertainties for emissions from other sectors in the Zheng et al. (2012) inventory were not quantified. The 95 % CI for the Zhang et al. (2009) inventory are ±208 % for EC and ±258 % for OC.

[b] Emissions and uncertainties were from M. He et al. (2011) for the inner PRD and from Streets et al. (2003b) for Hong Kong and Macau.

[c] The overall uncertainties (95 % CI) are shown in parentheses, calculated from sectorial emission uncertainties for residential sources (Zheng et al., 2012), for biomass burning (M. He et al., 2011), and for other anthropogenic sectors (Lei et al., 2011).

[d] Uncertainties are represented as ± standard deviations. The corresponding 95 % CI (calculated assuming normality) are shown in parentheses.





ACPD
15, 33583–33629, 2015



**Table 3.** VOC precursors of secondary organic carbon in the PRD area in 2006.

| VOC precursor | Emissions over the PRD area ($Gg\,yr^{-1}$) | | | | Simulated annual mean SOC concentrations ($\mu g\,C\,m^{-3}$)[d] | | | |
|---|---|---|---|---|---|---|---|---|
| | Anthropogenic[a] | Biomass burning[b] | Biogenic[c] | Total | Semi-volatile SOC | Non-volatile SOC | Dicarbonyl SOC | Total |
| Isoprene | 0.6 | 0.1 | 220 | 221 | 0.2 | 0.1 | 1.0 | 1.3 |
| Monoterpenes | 1.7 | 0.1 | 156 | 157 | 0.8 | 0.4 | < 0.1 | 1.2 |
| Alkanes | 113 | 0.1 | 0.9 | 114 | 0.1 | < 0.1 | – | 0.1 |
| Ethylene | 68.2 | 4.3 | 11.6 | 84.2 | – | – | 0.1 | 0.1 |
| Xylenes | 77.0 | 0.2 | 0.5 | 77.7 | 0.1 | 0.1 | 0.1 | 0.3 |
| Toluene | 51.7 | 0.1 | 0.2 | 52.0 | < 0.1 | < 0.1 | 0.1 | 0.1 |
| Acetone | 8.8 | 2.1 | 14.9 | 25.8 | – | – | < 0.1 | < 0.1 |
| Benzene | 18.7 | 0.5 | 0.1 | 19.3 | < 0.1 | < 0.1 | 0.1 | 0.1 |
| Acetylene | 16.6 | 0.1 | – | 16.7 | – | – | 0.1 | 0.1 |
| Propene | 6.5 | 0.7 | – | 7.1 | – | – | < 0.1 | < 0.1 |
| Glyoxal | 4.8 | 1.1 | – | 5.9 | – | – | 0.1 | 0.1 |
| Glycolaldehyde | 3.6 | 0.8 | – | 4.4 | – | – | < 0.1 | < 0.1 |
| Methylglyoxal | 3.2 | 0.7 | – | 3.9 | – | – | < 0.1 | < 0.1 |
| Hydroxyacetone | 3.0 | 0.7 | – | 3.7 | – | – | < 0.1 | < 0.1 |
| Cresols | < 0.1 | – | – | < 0.1 | – | – | < 0.1 | < 0.1 |
| Phenol | – | < 0.1 | – | < 0.1 | – | – | < 0.1 | < 0.1 |
| Sesquiterpenes | – | – | < 0.1 | < 0.1 | < 0.1 | < 0.1 | < 0.1 | < 0.1 |
| Total | 378 | 11 | 404 | 793 | 1.2 | 0.6 | 1.6 | 3.5 |

[a] Includes industry, power generation, transportation, and residential sources from the inventories developed by Zheng et al. (2012) and Zhang et al. (2009).
[b] From the inventories developed by M. He et al. (2011) and Streets et al. (2003b). Biomass burning emissions of glyoxal, methylglyoxal, glycolaldehyde, and hydroxyacetone were scaled from biomass burning CO emissions.
[c] Calculated in CMAQ using the MEGAN algorithm (Guenther et al., 2006).
[d] From CMAQ simulation using the top-down EC and OC emission estimates described in the text. SOC concentrations are averaged over urban and rural sites of available seasonal observations.





ACPD
15, 33583–33629, 2015



**Table 4.** List of the PRD area carbonaceous aerosol surface concentration measurements used in this study.

| Location | Aerosol size sampled | Filter accumulation period/sampling frequency | Observation period | Representative season | Observed seasonal mean surface concentrations [$\mu g C m^{-3}$] EC | OC | SOC | Method for EC and OC analysis[a] | Method for determining SOC | Reference[b] |
|---|---|---|---|---|---|---|---|---|---|---|
| Urban | | | | | | | | | | |
| Huangpu | $PM_{10}$ | 24 h/every 6 days | 01.2002–02.2002 | Winter | 12.1 | 32.6 | 15.0 | TOR | EC tracer[c] | [1] |
| (HP, 113.45° N, 23.10° E) | $PM_{10}$ | 24 h/daily | 06.2002–07.2002 | Summer | 10.5 | 28.5 | 15.8 | TOR | EC tracer | [2] |
| Liwan | $PM_{2.5}$ | 24 h/every 6 days | 10.2002,12.2002, 03.2003,06.2003 | Annual | 4.4 | 17.6 | 10.1 | TOT | EC tracer | [3] |
| (LW, 113.25° E, 23.12° N) | | | | | | | | | | |
| Longgui[d] | $PM_{10}$ | 24 h/every 6 days | 01.2002–02.2002 | Winter | 13.3 | 38.4 | 19.1 | TOR | EC tracer | [1] |
| (LG, 113.28° E, 23.27° N) | $PM_{10}$ | 24 h/daily | 06.2002–07.2002 | Summer | 8.8 | 24.7 | 14.1 | TOR | EC tracer | [2] |
| Luohu | $PM_{10}$ | 24 h/every 3 days | 01.2002–02.2002 | Winter | 7.3 | 16.4 | 5.8 | TOR | EC tracer | [1] |
| (LH, 114.12° E, 22.55° N) | $PM_{10}$ | 24 h/daily | 06.2002–07.2002 | Summer | 5.0 | 10.4 | 4.4 | TOR | EC tracer | [2] |
| Shenzhen graduate school Peking University | $PM_{2.5}$ | 24 h/every 6 days | 10.2002,12.2002, 03.2003,06.2003 | Annual | 3.9 | 11.1 | 4.5 | TOT | EC tracer | [3] |
| (PKU,113.93° E, 22.53° N) | $PM_1$ | –[e] | 10.2009–12.2009 | Autumn | 6.2 | 11.3 | 4.5 | – | AMS/PMF[f] | [4] |
| South China Institute | $PM_{2.5}$ | 24 h/daily | 01.2008–11.2008 | Winter | 7.9 | 24.2 | 15.9 | TOR | EC tracer | [5] |
| (SCI,113.15° E, 23.07° N) | $PM_{2.5}$ | 24 h/daily | 01.2008–11.2008 | Spring | 4.8 | 18.1 | 13.0 | TOR | EC tracer | [5] |
| | $PM_{2.5}$ | 24 h/daily | 01.2008–11.2008 | Summer | 4.7 | 14.0 | 9.0 | TOR | EC tracer | [5] |
| | $PM_{2.5}$ | 24 h/daily | 01.2008–11.2008 | Autumn | 5.3 | 23.6 | 18.0 | TOR | EC tracer | [5] |
| Sun Yat-sen University | $PM_{10}$ | 24 h/every 3 days | 01.2002–02.2002 | Winter | 8.1 | 23.3 | 11.6 | TOR | EC tracer | [1] |
| (SU, 113.28° E, 23.08° N) | $PM_{10}$ | 24 h/daily | 06.2002–07.2002 | Summer | 5.9 | 17.8 | 10.8 | TOR | EC tracer | [2] |
| | $PM_{2.5}$ | 24 h/every 6 days | 05.2005–07.2007 | Winter | 6.5 | 16.4 | 8.1 | TOR | EC tracer | [6] |
| | $PM_{2.5}$ | 24 h/every 6 days | 05.2005–07.2007 | Spring | 4.3 | 8.7 | 3.4 | TOR | EC tracer | [6] |
| | $PM_{2.5}$ | 24 h/every 6 days | 05.2005–07.2007 | Summer | 3.4 | 6.5 | 3.5 | TOR | EC tracer | [6] |
| | $PM_{2.5}$ | 24 h/every 6 days | 05.2005–07.2007 | Autumn | 5.5 | 11.0 | 5.9 | TOR | EC tracer | [6] |
| Xiangzhou | $PM_{10}$ | 24 h/every 3 days | 01.2002–02.2002 | Winter | 6.0 | 14.5 | 5.8 | TOR | EC tracer | [1] |
| (XZ, 113.57° E, 22.27° N) | $PM_{10}$ | 24 h/daily | 06.2002–07.2002 | Summer | 2.5 | 6.9 | 3.8 | TOR | EC tracer | [2] |
| Zhaoqing | $PM_{2.5}$ | 24 h/every 6 days | 08.2006–08.2007 | Winter | 4.8 | 9.4 | 3.2 | TOR | EC tracer | [6] |
| (ZQ, 112.45° E, 23.03° N) | $PM_{2.5}$ | 24 h/every 6 days | 08.2006–08.2007 | Spring | 3.4 | 6.5 | 2.7 | TOR | EC tracer | [6] |
| | $PM_{2.5}$ | 24 h/every 6 days | 08.2006–08.2007 | Summer | 3.0 | 5.7 | 1.2 | TOR | EC tracer | [6] |
| | $PM_{2.5}$ | 24 h/every 6 days | 08.2006–08.2007 | Autumn | 5.6 | 8.9 | 2.0 | TOR | EC tracer | [6] |

[a] TOR: thermal optical reflectance; TOT: thermal optical transmission; TMO: thermal manganese dioxide oxidation.
[b] [1] Cao et al. (2003), [2] Cao et al. (2004), [3] Hagler et al. (2006), [4] L.-Y. He et al. (2011), [5] Tao, J. personal communication (2012), [6] Ho, K.F. personal communication (2012), [7] Ho et al. (2003), [8] Hu et al. (2008), [9] Hu et al. (2012), [10] Huang et al. (2011), [11] Gnauk et al. (2008).
[c] SOC is calculated as OC – EC × (POC/EC), where the (POC/EC) value is obtained from the seasonal or annual minimum observed OC/EC ratio.
[d] Longgui was reported as a background site in Cao et al. (2003), but its EC and OC concentrations are very high and show obvious influence from local sources. We categorized it as an urban site for this study.
[e] Use AMS to collect organic matter (OM) and aethalometer to collect BC.
[f] The AMS measurements can be analyzed using the PMF technique to identify four OA components: HOA, BBOA, SV-OOA, and LV-OOA. We used the total oxygenated OA (SV-OOA + LV-OOA) as a surrogate for SOA.
[g] These sites were reported as background sites in Cao et al. (2003, 2004), Ho et al. (2003), Hagler et al. (2006), and Gnauk et al. (2008). We categorize them as rural sites for this study, because they reflect the baseline pollution levels in the PRD area.
[h] Use isoprene, monoterpenes, $\beta$-caryophyllene, and toluene as SOA tracers to estimate SOA concentration in $PM_{2.5}$ samples.





ACPD
15, 33583–33629, 2015



**Table 4.** Continued.

| Location | Aerosol size sampled | Filter accumulation period/sampling frequency | Observation period | Representative season | Observed seasonal mean surface concentrations [$\mu g C m^{-3}$] EC | OC | SOC | Method for EC and OC analysis[a] | Method for determining SOC | Reference[b] |
|---|---|---|---|---|---|---|---|---|---|---|
| Hong Kong | | | | | | | | | | |
| Baptist University (BU, 114.20° E, 22.32° N) | $PM_{10}$ | 24 h/every 6 days | 01.2002–02.2002 | Winter | 3.4 | 7.6 | 2.7 | TOR | EC tracer | [1] |
| | $PM_{10}$ | 24 h/daily | 06.2002–07.2002 | Summer | 3.9 | 6.7 | 2.0 | TOR | EC tracer | [2] |
| Central and western (CW, 114.13° E, 22.28° N) | $PM_{2.5}$ | 24 h/every 6 days | 10.2002,12.2002, 03.2003,06.2003 | Annual | 1.9 | 6.6 | 3.4 | TOT | EC tracer | [3] |
| Hok Tsui[g] (HT, 114.25° E, 22.22° N) | $PM_{10}$ | 24 h/every 6 days | 01.2002–02.2002 | Winter | 3.0 | 9.1 | 4.8 | TOR | EC tracer | [1] |
| | $PM_{10}$ | 24 h/daily | 06.2002–07.2002 | Summer | 1.1 | 4.1 | 2.8 | TOR | EC tracer | [2] |
| | $PM_{10}$ | 24 h/daily | 11.2000–02.2001 | Winter | 1.5 | 5.6 | – | TMO | – | [7] |
| Hong Kong University of Science and Technology (UST,114.25° E,22.33° N) | $PM_{2.5}$ | 24 h/every 2 days | 07.2006 | Summer | 1.0 | 4.7 | 4.1 | TOT | SOA tracer[h] | [8] |
| Kwun Tong (KT, 114.22° E, 22.30° N) | $PM_{10}$ | 24 h/daily | 11.2000–02.2001 | Winter | 5.1 | 10.4 | – | TMO | – | [7] |
| Tap Mun[g] (TM, 114.35° E, 22.47° N) | $PM_{2.5}$ | 24 h/every 6 days | 10.2002,12.2002, 03.2003,06.2003 | Annual | 0.8 | 4.9 | 3.5 | TOT | EC tracer | [3] |
| Tsuen Wan (TW, 114.10° E, 22.37° N) | $PM_{2.5}$ | 24 h/every 2 days | 07.2006 | Summer | 3.5 | 8.1 | 5.7 | TOT | SOA tracer | [8] |
| Tung Chung (TC, 113.93° E, 22.28° N) | $PM_{2.5}$ | 24 h/every 6 days | 10.2002,12.2002, 03.2003,06.2003 | Annual | 2.0 | 6.3 | 2.9 | TOT | EC tracer | [3] |
| | $PM_{2.5}$ | 24 h/every 2 days | 07.2006 | Summer | 1.6 | 5.5 | 5.0 | TOT | SOA tracer | [8] |
| Yuen Long (YL, 114.02° E, 22.43° N) | $PM_{2.5}$ | 24 h/every 2 days | 07.2006 | Summer | 2.4 | 7.8 | 4.9 | TOT | SOA tracer | [8] |
| Rural | | | | | | | | | | |
| Back Garden (BG, 113.03° E, 23.49° N) | $PM_{2.5}$ | 24 h/daily | 07.2006 | Summer | 3.3 | 5.7 | 2.0 | TOT | EC tracer | [9] |
| Conghua[g] (CH, 113.63° E, 23.63° N) | $PM_{2.5}$ | 24 h/every 6 days | 10.2002,12.2002, 03.2003,06.2003 | Annual | 1.4 | 9.1 | 6.7 | TOT | EC tracer | [3] |
| Kaiping (KP, 112.53° E, 22.32° N) | $PM_1$ | –[e] | 10.2008–11.2008 | Autumn | 2.2 | 6.3 | 4.7 | – | AMS/PMF[f] | [10] |
| Xinken[g] (XK, 113.58° E, 22.65° N) | $PM_{10}$ | 20 h/daily | 10.2004 | Autumn | 6.1 | 7.0 | 2.4 | – | EC tracer | [11] |
| Zhongshan (ZS, 113.41° E, 22.52° N) | $PM_{2.5}$ | 24 h/every 6 days | 10.2002,12.2002, 03.2003,06.2003 | Annual | 2.5 | 10.5 | 6.3 | TOT | EC tracer | [3] |

[a] TOR: thermal optical reflectance; TOT: thermal optical transmission; TMO: thermal manganese dioxide oxidation.
[b] [1] Cao et al. (2003), [2] Cao et al. (2004), [3] Hagler et al. (2006), [4] L.-Y. He et al. (2011), [5] Tao, J. personal communication (2012), [6] Ho, K.F. personal communication (2012), [7] Ho et al. (2003), [8] Hu et al. (2008), [9] Hu et al. (2012), [10] Huang et al. (2011), [11] Gnauk et al. (2008).
[c] SOC is calculated as OC – EC × (POC/EC), where the (POC/EC) value is obtained from the seasonal or annual minimum observed OC/EC ratio.
[d] Longgui was reported as a background site in Cao et al. (2003), but its EC and OC concentrations are very high and show obvious influence from local sources. We categorized it as an urban site for this study.
[e] Use AMS to collect organic matter (OM) and aethalometer to collect BC.
[f] The AMS measurements can be analyzed using the PMF technique to identify four OA components: HOA, BBOA, SV-OOA, and LV-OOA. We used the total oxygenated OA (SV-OOA + LV-OOA) as a surrogate for SOA.
[g] These sites were reported as background sites in Cao et al. (2003, 2004), Ho et al. (2003), Hagler et al. (2006), and Gnauk et al. (2008). We categorize them as rural sites for this study, because they reflect the baseline pollution levels in the PRD area.
[h] Use isoprene, monoterpenes, $\beta$-caryophyllene, and toluene as SOA tracers to estimate SOA concentration in $PM_{2.5}$ samples.





ACPD
15, 33583–33629, 2015



**Table 5.** Numbers of seasonal carbonaceous aerosol measurement sites in the PRD area used in this study.

| | Spring | Summer | Autumn | Winter | Total |
|---|---|---|---|---|---|
| Urban* | 6 | 10 | 6 | 10 | 32 |
| Rural | 2 | 3 | 4 | 2 | 11 |
| Total | 8 | 13 | 10 | 12 | 43 |

* All locations in Hong Kong are averaged to represent a single urban site, HK.





ACPD
15, 33583–33629, 2015



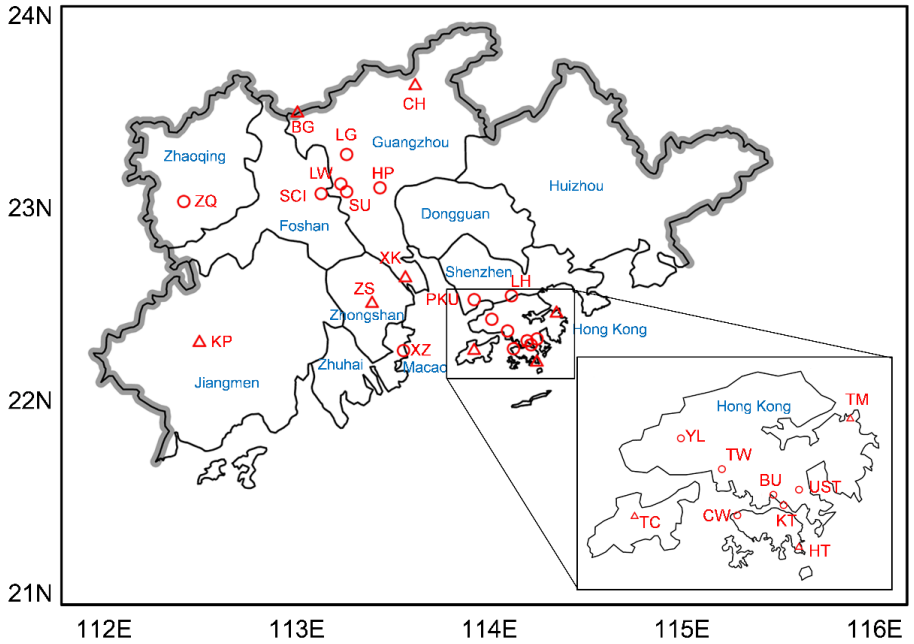


**Figure 1.** Locations of surface carbonaceous aerosol measurements used in this study, including 15 urban locations (circles) and 8 rural locations (triangles). Details of measurements at each location are presented in Table 4.





ACPD
15, 33583–33629, 2015



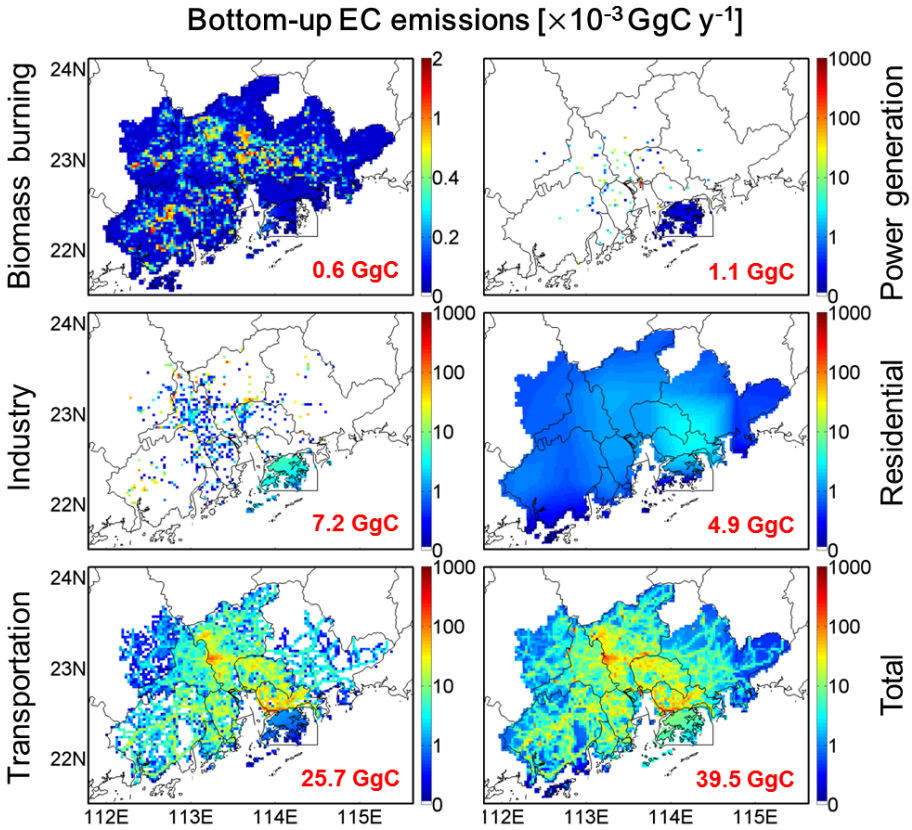


**Figure 2.** Annual emissions of EC in the PRD area in 2006 from the bottom-up inventories (Zheng et al., 2012; M. He et al., 2011; Zhang et al., 2009; and Streets et al., 2003b) used to drive our simulation. PRD annual emission totals are shown inset in red. For the sake of clarity, emissions outside the PRD area are not shown.





ACPD
15, 33583–33629, 2015



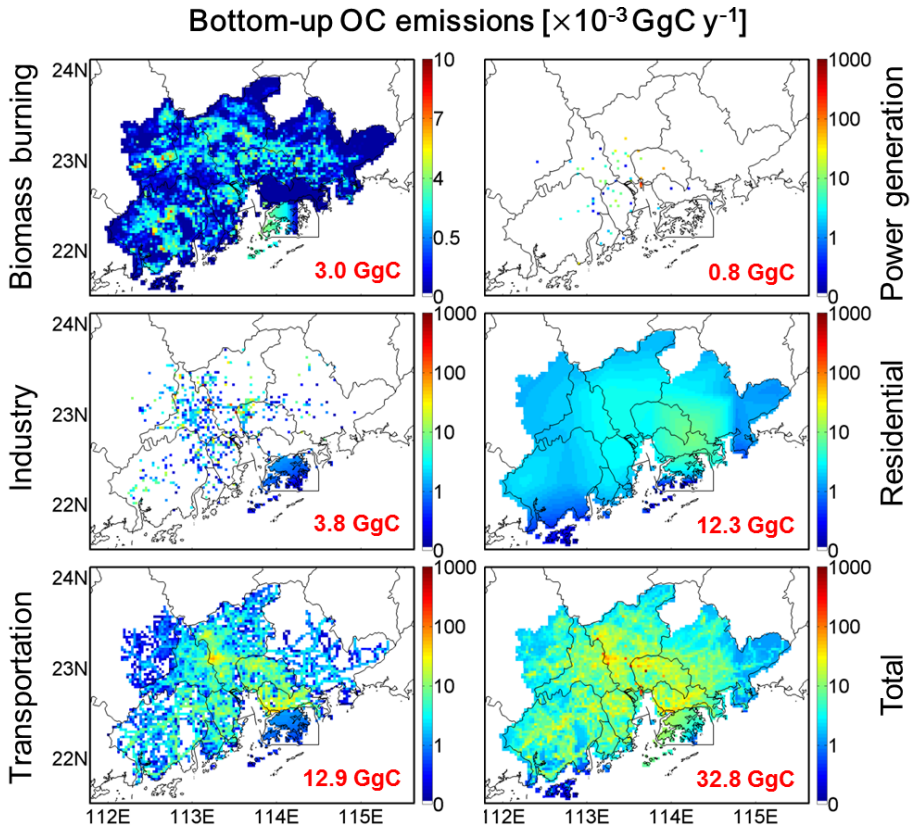


**Figure 3.** Annual emissions of OC in the PRD area in 2006 from the bottom-up inventories (Zheng et al., 2012; M. He et al., 2011; Zhang et al., 2009; and Streets et al., 2003b) used to drive our simulation. PRD annual emission totals are shown inset in red.





ACPD
15, 33583–33629, 2015



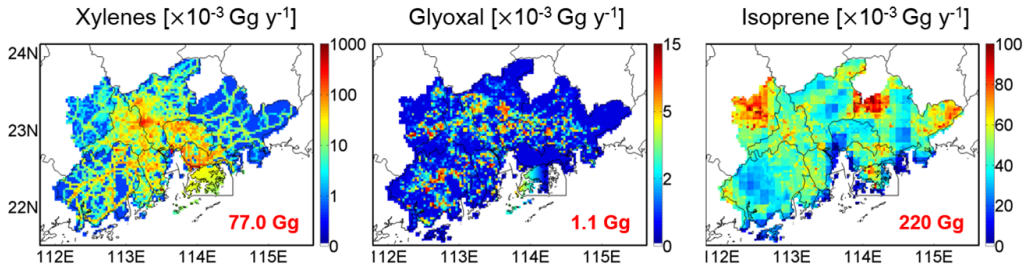


**Figure 4.** Annual emissions of anthropogenic xylenes, biomass burning glyoxal, and biogenic isoprene over the PRD area in 2006. PRD annual emission totals are shown inset in red.





ACPD
15, 33583–33629, 2015



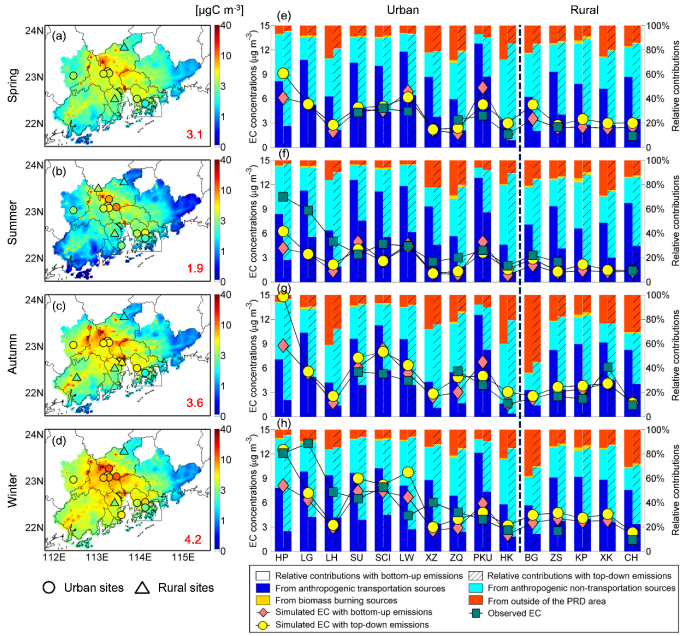


**Figure 5.** Seasonal mean surface EC concentrations and simulated source contributions at 15 urban and rural sites over the PRD area in 2006. The left panel shows seasonal mean observed surface EC concentrations at urban (circles) and rural (triangles) sites over the PRD area. Underlain are simulated seasonal mean EC concentrations in **(a)** spring, **(b)** summer, **(c)** autumn and **(d)** winter in 2006 using top-down emission estimates. Simulated PRD seasonal mean concentrations are shown inset in red. The right panel shows the simulated seasonal mean surface EC concentrations contributed by anthropogenic transportation sources (blue), anthropogenic non-transportation (industrial, power generation and residential) sources (cyan), biomass burning sources (yellow), and outside of the PRD area (orange) in **(e)** spring, **(f)** summer, **(g)** autumn and **(h)** winter in 2006 using the bottom-up and the top-down emission inventories. Also shown are observed EC concentrations (green squares), as well as simulated EC concentrations with bottom-up (pink diamonds) and top-down emissions (yellow circles).





ACPD
15, 33583–33629, 2015



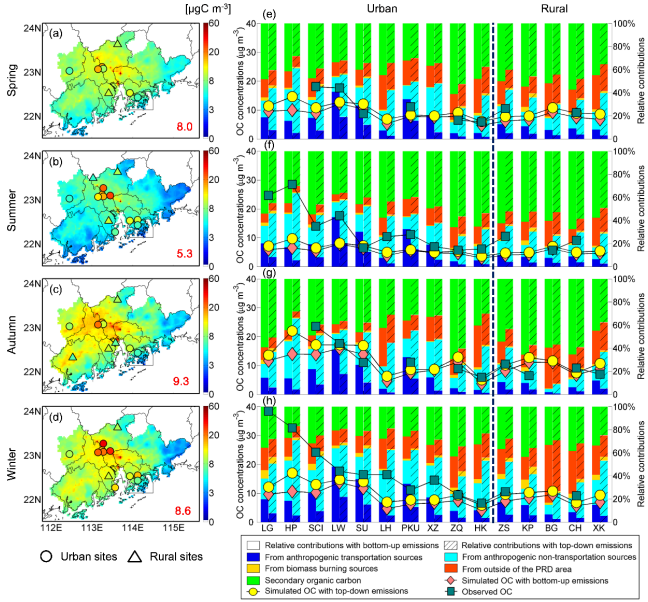


**Figure 6.** Seasonal mean surface OC concentrations and simulated source contributions at 15 urban and rural sites over the PRD area in 2006. The left panel shows seasonal mean observed surface OC concentrations at urban (circles) and rural (triangles) sites over the PRD area. Underlain are simulated seasonal mean OC concentrations in **(a)** spring, **(b)** summer, **(c)** autumn and **(d)** winter in 2006 using top-down emission estimates. Simulated PRD seasonal mean concentrations are shown inset in red. The right panel shows the simulated seasonal mean surface OC concentrations contributed by anthropogenic transportation sources (blue), anthropogenic non-transportation (industrial, power generation and residential) sources (cyan), biomass burning sources (yellow), outside of the PRD area (orange), and secondary sources (green) in **(e)** spring, **(f)** summer, **(g)** autumn and **(h)** winter in 2006 using the bottom-up and the top-down emission inventories. Also shown are observed OC concentrations (green squares), as well as simulated OC concentrations with bottom-up (pink diamonds) and top-down emissions (yellow circles).





ACPD
15, 33583–33629, 2015



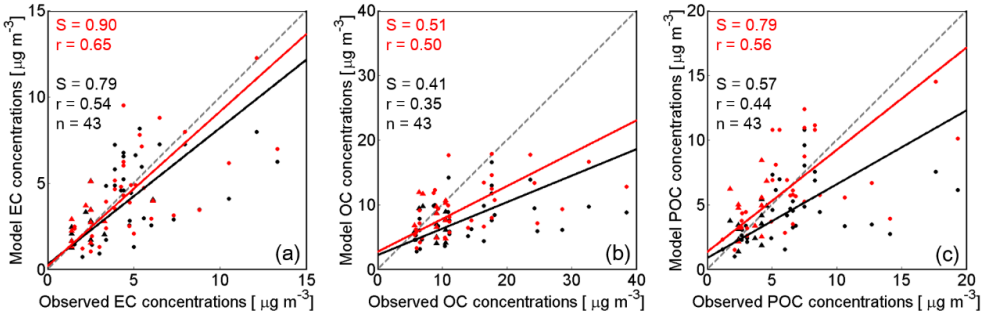


**Figure 7.** Simulated vs. observed seasonal surface **(a)** EC, **(b)** OC, and **(c)** POC concentrations at urban (circles) and rural (triangles) sites. Also shown are the reduced-major axis regression lines (solid lines): model results using bottom-up emission inventories (black), and model results using top-down emission estimates (red). The regression slopes ($S$), correlation coefficients ($r$), and numbers of data points ($n$) are shown inset. The grey dashed lines indicate the 1 : 1 lines.





ACPD
15, 33583–33629, 2015



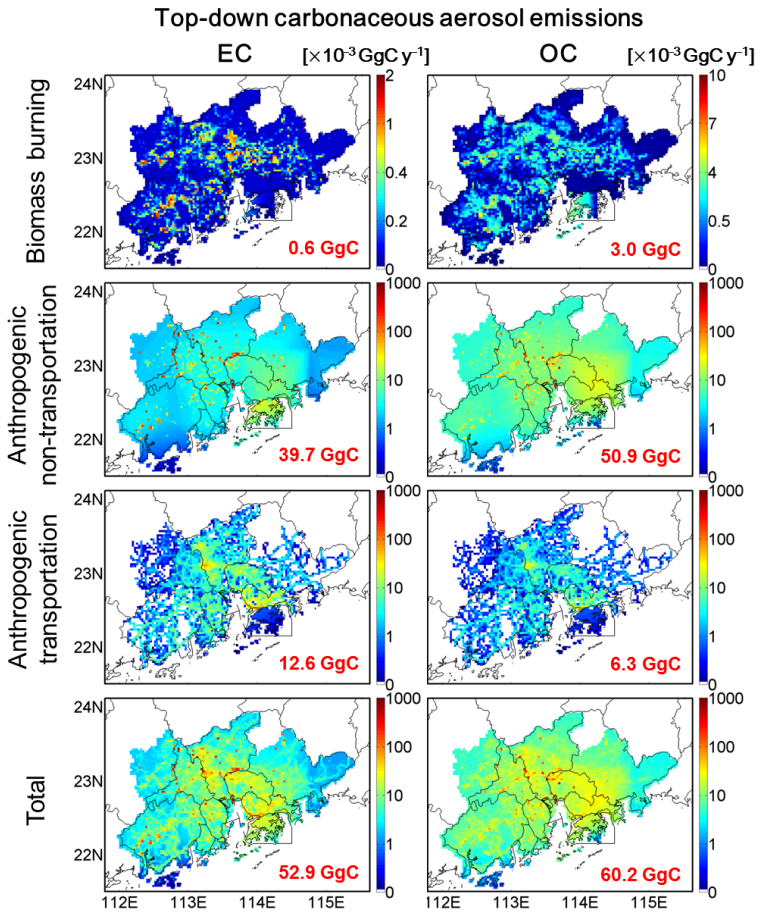


**Figure 8.** Top-down estimates of carbonaceous aerosol emissions in the PRD area in 2006. The annual emissions summed over the PRD area are shown inset in red.





ACPD
15, 33583–33629, 2015



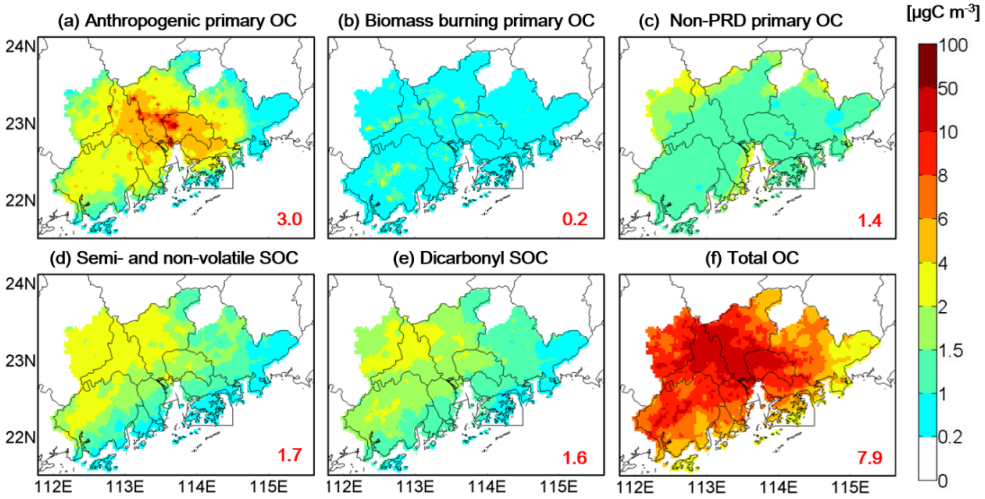


**Figure 9.** Simulated components of surface annual mean OC using top-down emission estimates: **(a)** anthropogenic primary OC; **(b)** biomass burning primary OC; **(c)** non-PRD primary OC (transport from outside of the PRD area); **(d)** semi-volatile and non-volatile oligomeric SOC from biogenic and anthropogenic VOC precursors; **(e)** SOC from irreversible uptake of dicarbonyls by aqueous-phase particles (mainly in clouds); and **(f)** total simulated OC. Simulated annual mean surface concentrations for each component are shown inset in red.





ACPD
15, 33583–33629, 2015